

Growth of Matter Perturbations in the Bi-Galileons Field Model

Khiredine Nouicer* and Hamza Boumaza†

*Laboratory of Theoretical Physics and Department of Physics,
Faculty of Exact and Computer Sciences,
University Mohamed Seddik Ben Yahia,
BP 98, Ouled Aissa, Jijel 18000, Algeria*
(Dated: December 2018)

We study a dark energy cubic bi-Galileons field model based on truncation of the recently proposed generalized covariant multi-Galileons model. We investigate the cosmological dynamic of the model by the theory of dynamical systems through the analysis of the properties of the fixed points in each cosmological epoch. We show the existence of two tracker solutions, one of which is that of the cubic single Galileon model and the other solution is the signature of the second Galileon field. Exploiting the competition between the two Galileon fields, we find a dark energy solution that avoids the approach to the tracker solution with dark energy equation of state $w_{DE} = -2$ during the matter epoch which is disfavored by the observational data. We study also the growth rate of matter perturbations. Using recent $f\sigma_8$ redshift space distortion (RSD) and model-independent observational Hubble (OHD) data sets, we place observational constraints on the coupling constant and cosmological parameters of the bi-Galileons model through Monte Carlo numerical method based on the Metropolis-Hastings algorithm. We find that the amplitude of growth matter fluctuations is consistent with the Planck15 data and ease the tension between early and later clustering, and fits better the data from the DES survey over the data from KiDS-450 survey. We also find that the best fit value for the Hubble constant is compatible with new measurements of Cepheid-supernovae distance scale. Finally, we perform a model selection through the Bayes factor and found that the bi-Galileons model is disfavored in comparison to the Λ CDM model, but slightly preferred to w CDM model.

PACS numbers: 04.50.Kd, 95.36.+x, 04.25.Nx, 98.80.Es

Keywords: Modified gravity theory; Dark energy; Cosmological perturbations; Hubble constant

I. INTRODUCTION

The origin of the late time accelerated expansion of the universe, discovered two decades ago [1], remains one of the theoretical challenging enigmas of modern cosmology. The observational data [2–4], obtained with high precision, of different cosmological parameters of the standard cosmological model, the Λ CDM model, have confirmed this fact, and that the accelerated expansion is driven by a dark energy (DE) component with an equation of state w_{DE} close to -1 . Even though the Λ CDM model has been successful in explaining the dynamics of the universe at large scales (particularly at the background level), it suffers from conceptual problems like *fine tuning*, *coincidence problem* and *the origin of dark energy* [5]. In fact, the Λ CDM model describes the dark energy component as a cosmological constant Λ , attributed to the vacuum energy density, but its value is extremely small compared to quantum field theory calculation [6]. Recently, two problems came to revive the debates about the theoretical foundations of the the Λ CDM model. The first one is the persistent tension between the values of Hubble constant H_0 constrained from the Cosmic Microwave Background (CMB) physics [3, 4] and local measurements from supernovae distance scale [7–9] and lensing time delays [10]. The second more debated problem of the Λ CDM model is the tension between the large $f\sigma_8$ values predicted by Planck/ Λ CDM data, indicating a high level of structure clustering, and the smaller values from the redshift space distortion (RSD) data obtained from galaxy redshift surveys in the late universe.

In order to solve these problems and particularly to account for the present accelerated expansion and the origin of dark energy driven it, alternative models have been introduced modeling the dark energy using scalar fields like: quintessence [11–14], k-essence [15, 16] and Brans-Dicke theories [17–19], Covariant Galileon [20, 21] and Kinetic Gravity Braiding [22, 23]. These models, which are large scale modification of general relativity, are actually known as sub-classes of the most general scalar-tensor theory with second order equations of motion, derived by Horndeski [24]. The current status of Horndeski’s theory and beyond is reviewed in [25]. In Horndeski theory, a rich variety of dark energy behaviors allow deviation from $w_{DE} = -1$ at the background level. As an example, the covariant Galileon model and its extension extensively studied and constrained in Ref.[26–34], showed the existence of a solution, known

* khnouicer@univ-jijel.dz

† boumaza14@yahoo.com

as tracker solution, that approach the Sitter solution at the late time universe. Despite its simplicity, this tracking solution is ruled out from the joint data analysis using Supernovae Ia (SNIa), Cosmic Microwave Background (CMB) and Baryon Acoustic Oscillation (BAO) [26] due to the bad behavior of the DE equation of state $w_{DE} = -2$ in the matter epoch. In addition, the insertion of nonlinear terms in the cubic Galileon action, such as the condensate Galileon model (CGM), modifies the evolution of DE equation of state and lead to a model favored over Λ CDM model by the criterion of Bayesian model selection [35, 36].

A recent alternative to scalar-tensor theory is the bi-scalar-tensor theory in which the action contains two scalar fields rather than one. These kinds of modified gravity models have been studied in the flat space-time at the background level [37, 38] and perturbed space-time [39]. Later, the generalized multi-Galileons was proposed as multi-fields generalization of Horndeski scalar-tensor theory following Horndeski's recipe, where all possible terms appearing in the second-order field equations of the bi-scalar-tensor theory was determined [40].

In the present paper, inspired by these approaches, we will present a sub-class of the multi-Galileons model, the bi-Galileons (BG) model, and investigate its cosmological evolution at the background and linear perturbed levels. We will show that the BG model can realize a variety of dark energy equation of state depending on the initial conditions of dynamical variables of the model. Particularly, we prospect the viability of the BG model in the light of the recent rate growth of matter perturbation data and Hubble parameter measurements and detect the signature of the second field in the cosmological behavior of the model.

The present paper is structured as follow. In Sec. II, we present the covariant BG model up to cubic term with constant coupling functions, and derive the main background field equations. In Sec. III, we study a simplified version of the BG model using the dynamical system approach through the introduction of suitable dimensionless variables. We perform a detailed analysis of the stability of the fixed points in each cosmological epoch, and investigate the existence of late-time attractor solutions. In Sec. IV we analyze the different cosmological implications of the fixed points on the behavior of the dark equation of state. Particularly, we focus on a dark energy solution with a dark energy equation of state close the Λ CDM model. In Sec. V we study the evolution of the growth rate of matter perturbations in the quasi-static approximation on sub-horizon scales, and compute the equations governing the evolution of perturbations. In Sec. VI we perform a parameter estimate using Monte Carlo analyses and confront our expectations with the Λ CDM and w CDM models. Finally, Sec.VII is devoted to conclusions.

II. THE BI-GALILEONS MODEL

We consider the following scalar-tensor modified model of gravity with two Galileons fields φ^I ($I = 1, 2$), labeled BG model, in a four-dimensional spacetime

$$S = \int d^4x \sqrt{-g} \left(\frac{R}{2} + a_{IJ} X^{IJ} - b_{KIJ} X^{IJ} \varphi_{;\mu}^{K;\mu} + \mathcal{L}_m + \mathcal{L}_r \right), \quad (1)$$

where R is Ricci scalar and the dimensionless constants a_{IJ} and b_{KIJ} ($I, J, K = 1, 2$) are symmetric in I, J . The Lagrangian \mathcal{L}_m and \mathcal{L}_r stands as usual for matter and radiation fields, respectively. The notation $X_{IJ} \equiv -\frac{1}{2} g^{\mu\nu} \partial_\mu \varphi^I \partial_\nu \varphi^J$ is the kinetic term for φ^I when $I = J$ and represents the coupling between the field velocities of the fields when $I \neq J$. The action (1) is a particular truncation of the more general covariant extension of the Galileon field model addressed in [41], and is invariant under the shift transformation $\varphi^I \rightarrow \varphi^I + \text{const.}$. The usual action for the cubic single Galileon field, labeled SG model, is recovered by setting $a_{2J} = 0$ and $b_{2JK} = 0$.

Varying the action with respect to the metric gives the field equations:

$$G_{\mu\nu} - a_{IJ} \varphi_{;\mu}^I \varphi_{;\nu}^J - b_{KIJ} \left(\varphi^{I;\alpha} \varphi_{;\mu}^J \varphi_{;\alpha\nu}^K + \varphi^{I;\alpha} \varphi_{;\nu}^J \varphi_{;\alpha\mu}^K - \varphi_{;\mu}^I \varphi_{;\nu}^J \varphi_{;\mu}^{K;\mu} \right) - g_{\mu\nu} \left(a_{IJ} X^{IJ} - b_{IJK} \varphi^{I;\alpha} \varphi^{J;\beta} \varphi_{;\alpha\beta}^K \right) = T_{\mu\nu}^{(m)} + T_{\mu\nu}^{(r)} \quad (2)$$

where $G_{\mu\nu}$ is the Einstein tensor and $T_{\mu\nu}^{(m)}$ and $T_{\mu\nu}^{(r)}$ are the matter and radiation energy-moment tensors, respectively. For a perfect fluid we have

$$T_{\mu\nu}^{(i)} = (\rho_i + P_i) u_\mu u_\nu + g_{\mu\nu} P_i, \quad (3)$$

where u_μ , ρ_i and P_i are the four velocity vector, energy density and pressure of the fluid, respectively. The energy-momentum conservation law is provided by

$$\nabla_\mu T^{(i)\mu\nu} = 0. \quad (4)$$

Now, varying the action (1) with respect to the scalar field φ^I leads to the appearance of third order derivative in the fields, which are canceled by imposing the constraint $b_{IJK} = b_{JKI}$. Then we are left with second order field equation

$$J_{I;\mu}^\mu = 0 \quad (5)$$

where

$$J_I^\mu = a_{IJ}\varphi^{J;\mu} - b_{IJK}(\varphi^{K;\mu}\square\varphi^J + X^{JK;\mu}). \quad (6)$$

We note the presence of first order derivative of φ^I which breaks the Galilean symmetry $\partial_\mu\varphi^I \rightarrow \partial_\mu\varphi^I + b_\mu$, $\varphi^I \rightarrow \varphi^I + c$.

Let us now study background cosmological solutions of the BG model. We consider the spatially flat Friedmann-Robertson-Walker (FRW) metric

$$ds^2 = -dt^2 + a(t)^2 \delta_{ij} dx^j dx^i, \quad (7)$$

where $a(t)$ is the scale factor. Substituting this ansatz in Einstein equations (2) we obtain the Friedmann equations

$$3H^2 = a_{IJ}X^{IJ} + 6b_{KIJ}HX^{IJ}\dot{\varphi}^K + \rho_m + \rho_r, \quad (8)$$

$$-(3H^2 + 2\dot{H}) = a_{IJ}X^{IJ} - 2b_{KIJ}X^{IJ}\dot{\varphi}^K + p_m + p_r, \quad (9)$$

where $H = \dot{a}/a$ is the Hubble parameter. From Eqs.(8) and (9), we identify the dark energy density and pressure as

$$\rho_{DE} = a_{IJ}X^{IJ} + 6b_{KIJ}HX^{IJ}\dot{\varphi}^K, \quad (10)$$

$$P_{DE} = a_{IJ}X^{IJ} - 2b_{KIJ}X^{IJ}\dot{\varphi}^K. \quad (11)$$

We also define the dark energy equation of state by

$$\omega_{DE} = \frac{P_{DE}}{\rho_{DE}} = \frac{a_{IJ}X^{IJ} - 2b_{KIJ}X^{IJ}\dot{\varphi}^K}{a_{IJ}X^{IJ} + 6b_{KIJ}HX^{IJ}\dot{\varphi}^K}. \quad (12)$$

It is clear that w_{DE} can cross the phantom divide line, $w_{DE} = -1$.

Inserting the metric (7) into (5), we obtain the scalar fields equations of motion

$$a_{IJ}(\ddot{\varphi}^J + 3H\dot{\varphi}^J) + 3b_{IJK}\left((3H^2 + \dot{H})\dot{\varphi}^J\dot{\varphi}^K + H\dot{\varphi}^{(K}\dot{\varphi}^{J)}\right) = 0, \quad (13)$$

where $\dot{\varphi}^{(K}\dot{\varphi}^{J)}$ stands for the corresponding symmetrized quantity.

III. DYNAMICAL ANALYSIS AND COSMOLOGICAL EVOLUTION

In this section we are interested by the homogeneous and isotropic cosmology of a simple version of the the model introduced in the last section. We consider a BG model where among the coupling constants in (1) we choose

$$a_{12} = a_{21} = b_{222} = 0. \quad (14)$$

For this model the Friedmann equations simplify to

$$3H^2 = \frac{a_{11}(\dot{\varphi}^1)^2}{2} + \frac{a_{22}(\dot{\varphi}^2)^2}{2} + 3H(b_{111}(\dot{\varphi}^1)^3 + 3b_{211}\dot{\varphi}^2(\dot{\varphi}^1)^2 + 3b_{122}(\dot{\varphi}^2)^2\dot{\varphi}^1) + \rho_m + \rho_r, \quad (15)$$

$$-(3H^2 + 2\dot{H}) = \frac{a_{11}(\dot{\varphi}^1)^2}{2} + \frac{a_{22}(\dot{\varphi}^2)^2}{2} - b_{111}(\dot{\varphi}^1)^2\ddot{\varphi}^1 - b_{211}(2\dot{\varphi}^2\dot{\varphi}^1\ddot{\varphi}^1 + (\dot{\varphi}^1)^2\ddot{\varphi}^2) - b_{122}(2\dot{\varphi}^2\dot{\varphi}^1\ddot{\varphi}^2 + (\dot{\varphi}^2)^2\ddot{\varphi}^1) + \frac{\rho_r}{3}. \quad (16)$$

where the density and pressure of dark energy are given by

$$\rho_{DE} = \frac{a_{11}(\dot{\varphi}^1)^2}{2} + \frac{a_{22}(\dot{\varphi}^2)^2}{2} + 3H(b_{111}(\dot{\varphi}^1)^3 + 3b_{211}\dot{\varphi}^2(\dot{\varphi}^1)^2 + 3b_{122}(\dot{\varphi}^2)^2\dot{\varphi}^1), \quad (17)$$

$$P_{DE} = \frac{a_{11}(\dot{\varphi}^1)^2}{2} + \frac{a_{22}(\dot{\varphi}^2)^2}{2} - b_{111}(\dot{\varphi}^1)^2\ddot{\varphi}^1 - b_{211}(2\dot{\varphi}^2\dot{\varphi}^1\ddot{\varphi}^1 + (\dot{\varphi}^1)^2\ddot{\varphi}^2) - b_{122}(2\dot{\varphi}^2\dot{\varphi}^1\ddot{\varphi}^2 + (\dot{\varphi}^2)^2\ddot{\varphi}^1), \quad (18)$$

and verify the continuity equation

$$\dot{\rho}_{DE} + 3H(\rho_{DE} + P_{DE}) = 0. \quad (19)$$

The BG fields equations of motion on the FRW background reads as

$$\begin{aligned} a_{11}(\ddot{\varphi}^1 + 3H\dot{\varphi}^1) + 3b_{111}\left(\left(3H^2 + \dot{H}\right)(\dot{\varphi}^1)^2 + 2H\ddot{\varphi}^1\dot{\varphi}^1\right) + 3b_{122}\left(\left(3H^2 + \dot{H}\right)(\dot{\varphi}^2)^2\right. \\ \left.+ 2H\ddot{\varphi}^2\dot{\varphi}^2\right) + 6b_{211}\left(\left(3H^2 + \dot{H}\right)\dot{\varphi}^1\dot{\varphi}^2 + H(\dot{\varphi}^2\ddot{\varphi}^1 + \dot{\varphi}^1\ddot{\varphi}^2)\right) = 0, \end{aligned} \quad (20)$$

$$\begin{aligned} a_{22}(\ddot{\varphi}^2 + 3H\dot{\varphi}^2) + 3b_{211}\left(\left(3H^2 + \dot{H}\right)(\dot{\varphi}^1)^2 + 2H\ddot{\varphi}^1\dot{\varphi}^1\right) + 6b_{122}\left(\left(3H^2 + \dot{H}\right)\dot{\varphi}^1\dot{\varphi}^2\right. \\ \left.+ H(\ddot{\varphi}^1\dot{\varphi}^2 + \dot{\varphi}^1\ddot{\varphi}^2)\right) = 0. \end{aligned} \quad (21)$$

The coupling between the two Galileons is controlled by the coefficients b_{111} , b_{122} and b_{211} . In order to reduce the dimension of the parameter space we assume the existence of de Sitter (dS) epoch where $H = H_{ds}$, $\dot{\varphi}^1 = \dot{\varphi}_{ds}^1 = u_{ds}$, and $\dot{\varphi}^2 = \dot{\varphi}_{ds}^2 = v_{ds}$, where H_{ds} , u_{ds} and v_{ds} are constants that can be fixed by the phase space properties of the model. During dS epoch, Eqs. (16), (20) and (21) are easily solved and lead to

$$a_{11} = 3 \frac{H_{ds}(2u_{ds}v_{ds}^2b_{122} - u_{ds}^2v_{ds}b_{211} - 2H_{ds})}{u_{ds}^2}, \quad a_{22} = -3 \frac{H_{ds}u_{ds}(2b_{122}v_{ds} + b_{211}u_{ds})}{v_{ds}}, \quad (22)$$

and

$$b_{111} = -\frac{3u_{ds}v_{ds}^2b_{122} + 3u_{ds}^2v_{ds}b_{211} - 2H_{ds}}{u_{ds}^3}. \quad (23)$$

A further reduction of the space of parameters is carried by imposing $a_{11} = 0$ and then solve for b_{122} to get

$$b_{111} = -\frac{1}{2} \frac{H_{ds}(2 + 3\alpha)}{u_{ds}^3}, \quad a_{22} = -6 \frac{H_{ds}^2}{v_{ds}^2} \quad (24)$$

where α is defined by $b_{211} = \frac{\alpha H_{ds}}{u_{ds}^2 v_{ds}}$. Further simplifications are obtained by the redefinition of the coupling parameters as

$$b_{211} \rightarrow b_{211} \frac{u_{ds}^2 v_{ds}}{H_{ds}} = \alpha, \quad b_{122} \rightarrow b_{122} \frac{u_{ds} v_{ds}^2}{H_{ds}} = 1 - \frac{\alpha}{2}, \quad (25)$$

$$b_{111} \rightarrow b_{111} \frac{u_{ds}^3}{H_{ds}} = -1 - \frac{3}{2}\alpha, \quad a_{22} \rightarrow a_{22} \frac{v_{ds}^2}{H_{ds}^2} = -6. \quad (26)$$

This redefinition does not affect the dynamics and allows us to hide the arbitrary parameters H_{ds} , u_{ds} and v_{ds} .

We now introduce the dimensionless variables

$$r_1 = (H\dot{\varphi}^1)^{-1}, \quad r_2 = H^{-1}(\dot{\varphi}^1)^3, \quad r_3 = \frac{\dot{\varphi}^2}{\dot{\varphi}^1}, \quad \Omega_m = \frac{\rho_m}{3H^2}, \quad \Omega_r = \frac{\rho_r}{3H^2}, \quad (27)$$

along with the notations

$$\epsilon_H = \frac{\dot{H}}{H^2}, \quad \epsilon_{\varphi^I} = \frac{\ddot{\varphi}^I}{H\dot{\varphi}^I}. \quad (28)$$

Solving Eqs.(27) we obtain

$$H = r_1^{-3/4} r_2^{-1/4}, \quad \dot{\varphi}^1 = \left(\frac{r_2}{r_1}\right)^{1/4}, \quad \dot{\varphi}^2 = r_3 \left(\frac{r_2}{r_1}\right)^{1/4}. \quad (29)$$

In terms of these variables, the Friedmann and the scalar field equations read as

$$4\epsilon_H + (r_3^2(\alpha - 2) - 4r_3\alpha + 3\alpha + 2) r_2\epsilon_{\varphi_1} + (2r_3(\alpha - 2) - 2\alpha) r_3r_2\epsilon_{\varphi_2} - 6r_1r_2r_3^2 + 2(\Omega_r + 3) = 0 \quad (30)$$

$$(3\alpha + 2 - 4r_3\alpha + r_3^2(\alpha - 2)) \epsilon_H + 2(2 - (2r_3 - 3)\alpha) \epsilon_{\varphi_1} - 2((2 - \alpha)r_3^2 + 2r_3\alpha) \epsilon_{\varphi_2} + 3r_3^2(\alpha - 2) - 12r_3\alpha + 9\alpha + 6 = 0 \quad (31)$$

$$((6 - 3\alpha)r_3 + 3\alpha) \epsilon_H + ((6 - 3\alpha)r_3 + 6\alpha) \epsilon_{\varphi_1} + (6 - 3\alpha - 6r_1) r_3\epsilon_{\varphi_2} - 9r_3(\alpha - 2) - 18r_3r_1 + 9\alpha = 0 \quad (32)$$

For completeness we solve these equations in terms of ϵ_H , ϵ_{φ_1} and ϵ_{φ_2}

$$\begin{aligned} \epsilon_H = & \frac{1}{\mathcal{D}} [(-9\alpha^3 + 54\alpha^2 - 108\alpha + (-18\alpha^2 + 72\alpha - 72)r_1 + 72)r_3^4 \\ & + (36\alpha^3 - 48\alpha r_1^2 - 144\alpha^2 + 144\alpha)r_3^3 \\ & + (-54\alpha^3 + 84\alpha^2 + 24\alpha + (72\alpha + 48)r_1^2 + (108\alpha^2 - 144\alpha - 144)r_1 + 48)r_3^2 \\ & + (36\alpha^3 + 48\alpha^2 + 48\alpha + (-144\alpha^2 - 96\alpha)r_1)r_3 + (54\alpha^2 + 72\alpha + 24)r_1 \\ & - 9\alpha^3 - 42\alpha^2 - 60\alpha - 24]r_2 + (4\alpha^2\Omega_r + 12\alpha^2 - 16\alpha\Omega_r - 48\alpha + 16\Omega_r + 48)r_3^2 \\ & + (-24\alpha^2 - 8\alpha^2\Omega_r + 16\alpha\Omega_r + (16\alpha\Omega_r + 48\alpha)r_1 + 48\alpha)r_3 + 48 + 12\alpha^2 + 4\alpha^2\Omega_r + 16\alpha\Omega_r \\ & + (-24\alpha\Omega_r - 72\alpha - 16\Omega_r - 48)r_1 + 48\alpha + 16\Omega_r] \end{aligned} \quad (33)$$

$$\begin{aligned} \epsilon_{\varphi_1} = & \frac{1}{\mathcal{D}} [((-12\alpha + 24)r_1^2 + (-6\alpha^2 + 24\alpha - 24)r_1)r_3^4 + (48\alpha r_1^2 + (48\alpha^2 - 96\alpha)r_1)r_3^3 \\ & + ((-36\alpha - 24)r_1^2 + (-78\alpha^2 + 72\alpha + 72)r_1)r_3^2 + (36\alpha^2 + 24\alpha)r_1r_3]r_2 \\ & + ((4\alpha\Omega_r + 36\alpha - 8\Omega_r - 72)r_1 - 2\alpha^2\Omega_r + 6\alpha^2 + 8\alpha\Omega_r - 24\alpha - 8\Omega_r + 24)r_3^2 \\ & + ((-16\alpha\Omega_r - 48\alpha)r_1 + 4\alpha^2\Omega_r - 12\alpha^2 - 8\alpha\Omega_r + 24\alpha)r_3 + (12\alpha\Omega_r - 36\alpha + 8\Omega_r - 24)r_1 \\ & - 2\alpha^2\Omega_r + 6\alpha^2 - 8\alpha\Omega_r + 24\alpha - 8\Omega_r + 24] \end{aligned} \quad (34)$$

$$\begin{aligned} \epsilon_{\varphi_2} = & -\frac{2}{\mathcal{D}} [(-6\alpha^2 + 24\alpha - 24)r_1r_3^4 + (30\alpha^2 - 60\alpha)r_1r_3^3 + (-69\alpha^2 + 12\alpha + 12)r_1r_3^2 \\ & + (72\alpha^2 + 48\alpha)r_1r_3 + (-27\alpha^2 - 36\alpha - 12)r_1]r_2 \\ & + 2(\alpha^2\Omega_r - 3\alpha^2 - 4\alpha\Omega_r + 12\alpha + 4\Omega_r - 12)r_3^2 \\ & + 2(-2\alpha^2\Omega_r + 6\alpha^2 + 4\alpha\Omega_r - 48\alpha r_1 - 12\alpha)r_3 \\ & + 2(72\alpha + 48)r_1 + 2\alpha^2\Omega_r - 6\alpha^2 + 8\alpha\Omega_r - 24\alpha + 8\Omega_r - 24] \end{aligned} \quad (35)$$

where

$$\begin{aligned} \mathcal{D} = & 2r_1(8(3\alpha - 2\alpha r_3 + 2) - r_2(r_3 - 1)^2(3\alpha - (\alpha - 2)r_3 + 2)^2) \\ & + ((\alpha + 2)^2 + (\alpha - 2)r_3((\alpha - 2)r_3 - 2\alpha))(r_2(3\alpha + 3(\alpha - 2)r_3^2 - 6\alpha r_3 + 2) - 8). \end{aligned} \quad (36)$$

Now, the cosmological dynamics of the model is studied by taking the derivative of the variables r_i , and Ω_r with respect to $N = \text{Ln } a$. Doing so we obtain

$$r_1' = -(\epsilon_{\varphi_1} + \epsilon_H)r_1, \quad (37)$$

$$r_2' = (3\epsilon_{\varphi_2} - \epsilon_H)r_2, \quad (38)$$

$$r_3' = (\epsilon_{\varphi_2} - \epsilon_{\varphi_1})r_3, \quad (39)$$

$$\Omega_r' = -2(2 + \epsilon_H)\Omega_r. \quad (40)$$

For our purpose we just consider Eq.(39) with the relations (33)-(35) to get

$$r_3' = \frac{2}{\mathcal{D}} r_1 r_3 (r_3 - 1) ((\alpha - 2)r_3 - 3\alpha - 2) (3r_2(2 + 3\alpha - 6\alpha r_3 + (3\alpha + 2r_1 - 6)r_3^2) - 2(\Omega_r + 9)). \quad (41)$$

In terms of the variables r_i the dark energy density and the dark energy equation of state are given by

$$\Omega_{DE} = -\frac{1}{2} r_2 (r_3^2 (2r_1 + 3\alpha - 6) - 6r_3\alpha + 3\alpha + 2), \quad (42)$$

$$w_{DE} = \frac{3 + 2\epsilon_H + \Omega_r}{\Omega_{DE}}. \quad (43)$$

We also define the effective equation of state, $\omega_{eff} = -1 - \frac{2}{3}\epsilon_H$. Setting $r_3 = 1$ in (42) it follows that the dark energy density of the BG model is proportional to that of the cubic SG model, $\Omega_{DE}^{BG} = r_1^2 \Omega_{DE}^{SG}$. This means that two models are governed by the same dynamics, and we expect to find a tracker solution similar to that of the cubic SG model.

The fixed points $(r_{1c}, r_{2c}, r_{3c}, \Omega_{rc})$ of the BG model are solutions of the equations $r'_i = 0$ and $\Omega'_r = 0$. However, we need also to identify the stability of these fixed points by calculating the matrix of the coefficients of the perturbed equations to linear order. A critical point is said to be stable only if all the eigenvalues of the perturbation matrix are negatives, unstable if the eigenvalues are positives and saddle if the eigenvalues have different signs. By inspection, Eq. (41) admits two fixed points given by

$$r_3 = 1, \quad \text{and} \quad r_3 = \frac{3\alpha + 2}{\alpha - 2}.$$

These solutions signal the existence of two tracker solutions. There is also an other solution given by $r_1 = 0$ which gives the so-called small regime. In Table.I, we list the fixed points, the conditions of their existence and their stability in the radiation, matter and de Sitter epochs. The interesting fact is the emergence of two sets of fixed points in each cosmological epoch. The first set of fixed points, independent of the coupling constant α , is an extension of the one found in the context of the SG field model, while the second set of fixed points is intrinsic to the cubic BG model and may induce a new behavior of dark energy equation of state, particularly in the matter dominated epoch.

Point	r_{1c}	r_{2c}	r_{3c}	Ω_r	Existence	eigenvalues	Stability	ω_{eff}	Ω_m
A	0	0	r_3	1	$((\alpha + 2)^2 - 2(2 - \alpha)\alpha r_3 + (2 - \alpha)^2 r_3^2) \neq 0$	$(0, 0, \frac{5}{2}, \frac{1}{2})$	Unstable	$\frac{1}{3}$	0
B	0	0	r_3	0	$((\alpha + 2)^2 - 2(2 - \alpha)\alpha r_3 + (2 - \alpha)^2 r_3^2) \neq 0$	$(0, 0, \frac{9}{4}, -\frac{3}{4})$	Saddle	0	1
C	1	0	1	1	$(\alpha + 2) \neq 0$	$(0, 8, -5, -5)$	Saddle	$\frac{1}{3}$	0
D	1	0	1	0	$(\alpha + 2) \neq 0$	$(0, 6, -\frac{9}{2}, -\frac{9}{2})$	Saddle	0	1
T1	1	1	1	0	$(\alpha + 2) \neq 0$	$(0, -3, -3, -3)$	Stable	-1	0
E	$-\frac{(\alpha+1)(\alpha-2)}{3\alpha+2}$	0	$\frac{3\alpha+2}{\alpha-2}$	1	$(\alpha + 1)(\alpha + 2)(\alpha - 2)(3\alpha + 2) \neq 0$	$(0, 8, -5, -5)$	Saddle	$\frac{1}{3}$	0
F	$-\frac{(\alpha+1)(\alpha-2)}{3\alpha+2}$	0	$\frac{3\alpha+2}{\alpha-2}$	0	$(\alpha + 1)(\alpha + 2)(\alpha - 2)(3\alpha + 2) \neq 0$	$(0, 6, -\frac{9}{2}, -\frac{9}{2})$	Saddle	0	1
T2	$-\frac{(\alpha+1)(\alpha-2)}{3\alpha+2}$	$-\frac{\alpha-2}{(3\alpha+2)(\alpha+1)}$	$\frac{3\alpha+2}{\alpha-2}$	0	$(\alpha + 1)(\alpha + 2)(\alpha - 2)(3\alpha + 2) \neq 0$	$(0, -3, -3, -3)$	Stable	-1	0

TABLE I. Fixed points of the BG model, their stability and existence conditions.

IV. ANALYSIS OF THE FIXED POINTS

A. Small regime

The fixed points **A** and **B** are radiation and matter dominated points and constitute the regime for which $r_1, r_2 \ll 1$. A series expansion in r_1 and r_2 lead to the simplified dynamical equations

$$r'_1 = \frac{(\Omega_r + 9)}{4} r_1, \quad (44)$$

$$r'_2 = \frac{(5\Omega_r - 3)}{4} r_2, \quad (45)$$

$$r'_3 = \frac{r_1 r_3 (r_3 - 1) ((\alpha - 2) r_3 - 3\alpha - 2) (\Omega_r + 9)}{2 [(\alpha - 2)^2 r_3^2 - 2\alpha(\alpha - 2) r_3 + (\alpha + 2)^2]}, \quad (46)$$

$$\Omega'_r = \Omega_r \left[(\Omega_r - 1) + \frac{3}{8} r_2 ((\alpha - 2) r_3^2 - 3\alpha (2r_3 - 1) + 2) (\Omega_r - 3) \right]. \quad (47)$$

In the small regime the effective EoS and dark energy parameters are given by

$$\omega_{eff} \approx \frac{\Omega_r}{3} + \frac{1}{8} \left[(\alpha - 2) r_3^2 - 2\alpha r_3 + \alpha + \frac{2}{3} \right] (\Omega_r - 3) r_2 \quad (48)$$

$$\begin{aligned} \omega_{DE} \approx & -\frac{1}{12} (\Omega_r - 3) + \frac{1}{3} \left[\frac{\Omega_r + 9}{3(\alpha - 2) r_3^2 - 6\alpha r_3 + 3\alpha + 2} \right] r_1 r_3^2 \\ & - \frac{1}{96} (\Omega_r - 3) (3(\alpha - 2) r_3^2 - 6\alpha r_3 + 3\alpha + 2) r_2. \end{aligned} \quad (49)$$

In the radiation and matter dominated epochs we obtain $\omega_{DE} = 1/6$ and $\omega_{DE} = 1/4$, respectively. Integration of Eqs.(44) and (45) in the radiation and matter eras give $r_1 \propto a^{5/2}$, $r_2 \propto a^{1/2}$ and $r_1 \propto a^{9/4}$, $r_2 \propto a^{-3/4}$, respectively. Substituting in Hubble parameter $H(t)$ given by (29) we obtain, as expected, $H(t) \propto a^{-2}$ ($H(t) \propto a^{-3/2}$) in the radiation epoch (matter epoch). In the limit of large r_3 , Eq.(46) is easily integrated and gives $r_3 \propto \exp\left(\frac{2a^\sigma}{\alpha-2}\right)$ where $\sigma = 5/2$ ($\sigma = 9/4$) in the radiation (matter) epoch. Translating these results in terms of the field velocity we get $\dot{\varphi}^1 \propto t^{-1/4}$, $\dot{\varphi}^2 \propto t^{-1/4} \exp\left(\frac{2t^{5/4}}{\alpha-2}\right)$ in the radiation epoch, and $\dot{\varphi}^1 \propto t^{-1/2}$, $\dot{\varphi}^2 \propto t^{-1/2} \exp\left(\frac{2t^{3/2}}{\alpha-2}\right)$ in the matter epoch. Hence the evolution $\dot{\varphi}^1$ of $\dot{\varphi}^2$ is slower than that of the tracker solutions, $\{\dot{\varphi}^1, \dot{\varphi}^2\} \propto t$. We note that to maintain r_3 large in the radiation and matter epochs we must impose a large initial condition on r_3 and then the evolution of the field φ^1 is slower than that of φ^2 .

B. de Sitter fixed points

As we can see from table I we have two stable de Sitter fixed points **T1** and **T2**. The fixed point **T1** is the same as the one already found in the context of the SG model and discussed extensively in . The second de Sitter fixed point **T2** is considered as the signature of the BG model. Assuming that the coordinates of the fixed point **I** are all positive lead to the following condition on the coupling constant

$$\alpha < -1. \quad (50)$$

We show that the Hubble parameter and field velocity in dS epoch are given by

$$H_{ds}^{(T1)} = 1, \quad \dot{\varphi}_{ds}^{1(T1)} = \dot{\varphi}_{ds}^{2(T1)} = 1, \quad (51)$$

$$H_{ds}^{(T2)} = \left| \frac{(3\alpha + 2)}{(\alpha - 2)(\alpha + 1)^{1/2}} \right|, \quad \dot{\varphi}_{ds}^{1(T2)} = \left| \frac{1}{(\alpha + 1)^{1/2}} \right|, \quad \dot{\varphi}_{ds}^{2(T2)} = H_{ds}^{(T2)}. \quad (52)$$

This implies that during the de Sitter epoch (**T2**) the variation of the field φ^2 is slower than that of the field φ^1 for $-2 < \alpha < -1$.

From the definition of r_1 and r_2 in (27), the dS fixed points allow for tracker solutions such that $\dot{\varphi}_I^{(j)} H = C_I^{(j)}$ where $I = 1, 2$, $j = \mathbf{T1}, \mathbf{T2}$ and $C_I^{(j)}$ are constants which can be determined from (51) and (52).

Let us consider the radiation and matter dominated epochs (**C**, **D**, **E**, and **F** fixed points) and expand the dynamical equations to first order in r_2 to obtain along the tracker **T1**

$$r_2' = \frac{2r_2(\Omega_r - 3r_2 + 3)}{r_2 + 1} \quad (53)$$

$$\Omega_r' = \frac{\Omega_r(\Omega_r - 7r_2 - 1)}{r_2 + 1} \quad (54)$$

and

$$r_2' = - \frac{2r_2((\alpha - 2)\Omega_r + 3(\alpha + (3\alpha^2 + 5\alpha + 2)r_2 - 2))}{-\alpha + (3\alpha^2 + 5\alpha + 2)r_2 + 2} \quad (55)$$

$$\Omega_r' = - \frac{\Omega_r(-\alpha + (\alpha - 2)\Omega_r + 7(3\alpha^2 + 5\alpha + 2)r_2 + 2)}{(-\alpha + (3\alpha^2 + 5\alpha + 2)r_2 + 2)} \quad (56)$$

for the tracker **T2**.

We note that the evolution of r_2 and Ω_r along the tracker solution **T2** is a function of the coupling constant α , while along the tracker **T1** we have exactly the evolution equations of Ref. [26]. The set of equations (53-54) and (55-56) can be written in compact form

$$r_2' = \frac{2r_2 \left(\Omega_r + 3 - 3\Omega_{DE}^{(i)} \right)}{\Omega_{DE}^{(i)} + 1}, \quad (57)$$

$$\Omega_r' = \frac{\Omega_r \left(\Omega_r - 7\Omega_{DE}^T - 1 \right)}{\Omega_{DE}^{(i)} + 1}. \quad (58)$$

where

$$\Omega_{DE}^{(i)} = \frac{r_2}{r_{2c}^{(i)}}. \quad (59)$$

and $r_{2c}^{(\mathbf{T1})} = 1$ and $r_{2c}^{(\mathbf{T2})} = -\frac{\alpha-2}{(3\alpha+2)(\alpha+1)}$. As long as $\alpha < -1$, $\Omega_{DE}^{(\mathbf{T})}$ remains positive. In dS epoch we have $\Omega_{DE} = 1$ along the two trackers.

Combining Eqs.(57) and (58), we show that

$$\frac{r_2'}{2r_2} - \frac{\Omega_r'}{\Omega_r} = 4. \quad (60)$$

The integration of this equation with respect to N gives ($a = e^N$) :

$$r_2 = d^{(i)} a^8 \Omega_r^2. \quad (61)$$

where $d^{(i)}$ is a constant given by $d^{(\mathbf{T1})} = \frac{1-\Omega_m^{(0)}-\Omega_r^{(0)}}{(\Omega_r^{(0)})^2}$, and $d^{(\mathbf{T2})} = -\frac{\alpha-2}{(3\alpha+2)(\alpha+1)}d^{(\mathbf{T1})}$. Using Eq.(61) and $\Omega_r = (H_0/H)^2 \Omega_r^{(0)} a^{-4}$, $\Omega_m = (H_0/H)^2 \Omega_m^{(0)} a^{-3}$ in (58), and solving for Ω_r , we finally obtain the Hubble parameter along both the trackers

$$\left(\frac{H}{H_0} \right)^2 = \frac{1}{2} \Omega_m^{(0)} (z+1)^3 + \frac{1}{2} \Omega_r^{(0)} (z+1)^4 + \sqrt{1 - \Omega_m^{(0)} - \Omega_r^{(0)} + \left(\Omega_m^{(0)} (z+1)^3 + \Omega_r^{(0)} (z+1)^4 \right)^2}. \quad (62)$$

This equation does not show any dependence on the coupling α , and is exactly the one obtained on the SG field model Ref. [26]. On the other hand, the effective equation of state w_{eff} and dark energy equation of state w_{DE} on the tracker solutions are given by

$$w_{eff}^{(j)} = \frac{\Omega_r - 6\Omega_{DE}^{(j)}}{3 \left(1 + \Omega_{DE}^{(j)} \right)}, \quad w_{DE}^{(j)} = -\frac{\Omega_r + 6}{3 \left(1 + \Omega_{DE}^{(j)} \right)}. \quad (63)$$

In the early cosmological epoch in which $\Omega_{DE}^{(i)} \ll 1$ these relations reduce to $w_{eff} \simeq \Omega_r/3$ and $w_{DE} \simeq -2 - \Omega_r/3$. Then, in the radiation epoch ($\Omega_{DE}^{(j)} \ll 1$ and $\Omega_r \approx 1$) we have $w_{eff} \simeq 1/3$ and $w_{DE} \simeq -7/3$, while in matter epoch ($\Omega_{DE}^{(j)} \ll 1$ and $\Omega_r \ll 1$) we have $w_{eff} \simeq 0$ and $w_{DE} \simeq -2$. In dS epoch we obtain $w_{eff} = -1$ and $w_{DE} = -1$. Although the dynamical evolution of r_2 and Ω_r is different along the trackers **T1** and **T2**, we found that the evolution of the dark energy equation of state along the tracker solutions of the BG field model is identical to that of SG field model, and then is also plagued by the same bad behavior in the matter epoch, where it reaches the value $w_{DE} = -2$. Hence, the tracker solution of the BG model is in tension with cosmological data with respect to the Λ CDM model [26].

C. Dark energy solution

The dynamical variable r_3 allows us to investigate deeply the competition between the fields of the BG model since this variable controls the rate of the evolution of the field φ^2 with to the field φ^1 . Indeed, besides the solutions listed in table. I, the dynamical equations exhibit a rich dark energy structure in the case where r_3 dominates over r_1 and

r_2 in the radiation and matter epochs. We also choose r_2 much smaller than 1 to maintain $\Omega_{DE} \ll 1$ in these epochs. In this regime the dynamical system reduce to

$$r_1' \approx \frac{1}{4} \frac{r_1 (\Omega_r + 9) (\alpha + 2r_1 - 2)}{\alpha - 2}, \quad (64)$$

$$r_3' \approx \frac{(\Omega_r + 9) r_1 r_3}{2(\alpha - 2)}, \quad (65)$$

$$\Omega_r' \approx \Omega_r (\Omega_r - 1). \quad (66)$$

Integrating Eqs.(64) and (65) we obtain

$$r_1(a) = \frac{(\alpha - 2) a^\sigma}{B(\alpha - 2) - 2a^\sigma}, \quad r_3(a) = \frac{A}{2a^\sigma - B(\alpha - 2)} \quad (67)$$

where A and B are constants of integration and $\sigma = 5/2$, $\sigma = 9/4$ for $\Omega_r = 1$ and $\Omega_r = 0$, respectively. It is clear that $r_1 = (2 - \alpha)/2$ is one solution of Eq.(64). We have to choose $B \approx 0$ and $A \approx 1$ to maintain the dominance of r_3 over r_1 and r_2 . Then, we are left with the following new solution $\mathbf{J}_{\Omega_r} = (r_1 = (2 - \alpha)/2, r_2 \approx 0, r_3 \gg 1, \Omega_r)$. Along this solution the effective and dark energy equations of state do not dependent on the coupling constant α and are given by

$$w_{eff} \approx \frac{\Omega_r}{3}, \quad w_{DE} \approx -\frac{1}{2} - \frac{\Omega_r}{6}. \quad (68)$$

This approximate solution (68) is not accurate in dS epoch. The behavior of the w_{DE} along the dark energy solution is slightly improved compared to that along the tracker solutions **T1** and **T2**. In fact, during radiation and matter dominated epochs we have $w_{DE} = -2/3$ and $w_{DE} = -1/2$, respectively. This means that the cosmological dynamics with initial conditions $r_3^{(s)}$ much larger than 1 escape the tracker curves with $w_{DE} = -2$ during matter dominated epoch. In terms of the field velocity we obtain $H\dot{\varphi}^1 = \frac{B(\alpha-2)-2a^\sigma}{(\alpha-2)a^\sigma}$ and $H\dot{\varphi}^2 = \frac{A}{(\alpha-2)a^\sigma}$. For $B \approx 0$ we get $H\dot{\varphi}^1 = \text{constant}$. We then obtain $\dot{\varphi}^1 \propto t$, $\dot{\varphi}^2 \propto t^{9/4}$ and $\dot{\varphi}^1 \propto t$, $\dot{\varphi}^2 \propto t^{5/2}$ in radiation and matter epochs, respectively. These behaviors show the dominance of the field φ^2 over φ^1 during these epochs. A second solution to Eqs. (64) and (65) is $r_1 = 0$, $r_2 = 0$ which is already given by the fixed points **A** and **B**, and for which we have $w_{eff} \approx \frac{\Omega_r}{3}$, $w_{DE} \approx \frac{1}{4} - \frac{\Omega_r}{12}$.

We proceed now to a numerical integration of equations of the BG model considering two cases. The first case, labeled BG1 model, corresponds to the integration of the full set of dynamical equations (37-40), and the second case, labeled BG2 model, is based on the integration of the dark energy solution found in Sec. IVC. In Fig. 1, we plot the evolution of the dimensionless energy densities for the BG1 and BG2 models with that of the tracker solutions and compare with the energy density evolution in the Λ CDM model. We start the simulation at early times in the deep radiation epoch at $N^{(s)} = -20$ ($z^{(s)} \approx 4.85 \times 10^8$). The initial conditions on $r_i^{(s)}$ are chosen such that the today values of the energy densities are compatible with the Planck 2015 data (TT+lowE), $\Omega_m = 0.315$ and $\Omega_{DE} = 0.685$. We observe that the evolution in the BG models is compatible with that of the Λ CDM model, whereas the evolution of the energy densities obtained from the tracker solutions is not, particularly the tracker solution **T1**. An other observation is that the BG models follow the tracker solution **T2** earlier or later depending on the initial conditions. In fact, this approach to the tracker **T2** is best seen in Fig. 2 where we show the evolution of the dark energy parameter of state w_{DE} . Indeed, w_{DE} follows the tracker curve early at moderate initial condition $r_3^{(s)}$ for the BG1 and BG2 models. The difference between the two models occurs at around $a < 6 \times 10^{-3}$ where the w_{DE} follow two different paths in the radiation epoch and at the onset of the matter epoch. For $a > 6 \times 10^{-3}$, w_{DE} reaches the value $-1/2$, as predicted by the dark energy solution (68), before decreasing to values around -1 at the onset of the dS epoch. We observe also that a large initial condition on r_3 is the best realization for w_{DE} which becomes very close to $w_{DE} = -1$. Finally, we note that large initial conditions $r_3^{(s)}$ does not necessarily imply large present-day values on r_i , as we obtain for the red curve shown in Fig. 2 the following values: $r_1^{(0)} = 6.0185$, $r_2^{(0)} = 0.0125$ and $r_3^{(0)} = 2.9824$. We conclude that the tracker solutions are incompatible with Λ CDM model in the matter dominated epoch, and that the evolution of w_{DE} calculated from the dark energy solution in the regime of $r_3^{(s)} \gg \{1, r_1^{(s)}\}$ and $r_2^{(s)} \ll 1$ prevents the approach to the bad behavior of the tracker in the matter epoch. A similar behavior has been recently obtained with the Galileon ghost condensate model [35, 36].

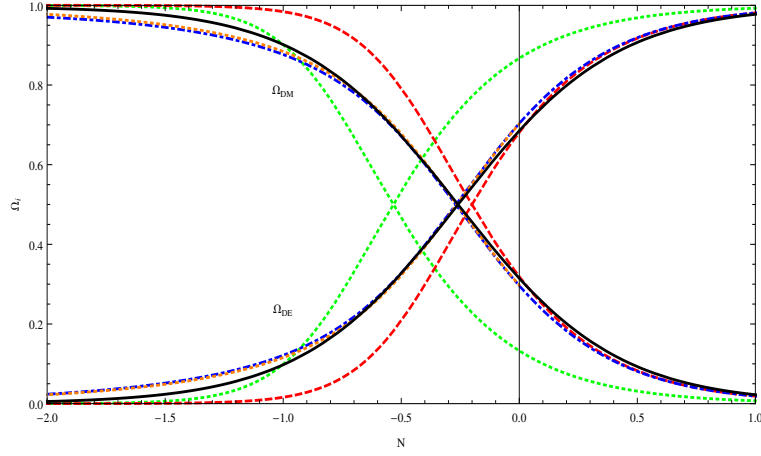


FIG. 1. Evolution of energy densities for BG and Λ CDM models. For all the plots we take $\alpha = -19.8$ and $\Omega_m^{(0)} h^2 = 0.1426$ (Planck 2015: TT+lowE). The initial conditions for BG1 model are: $r_1^{(s)} = 5.5 \times 10^{-14}$, $r_2^{(s)} = 1.348 \times 10^{-22}$ and $r_3^{(s)} = 3 \times 10^6$ (Blue), and $r_1^{(s)} = (2 - \alpha)/2$, $r_2^{(s)} = 5 \times 10^{-62}$, $r_3^{(s)} = 2.4 \times 10^{20}$ (Orange) for BG2 model. The curves for tracker solutions **T1** and **T2** and Λ CDM model are shown by green, red and black colors, respectively.

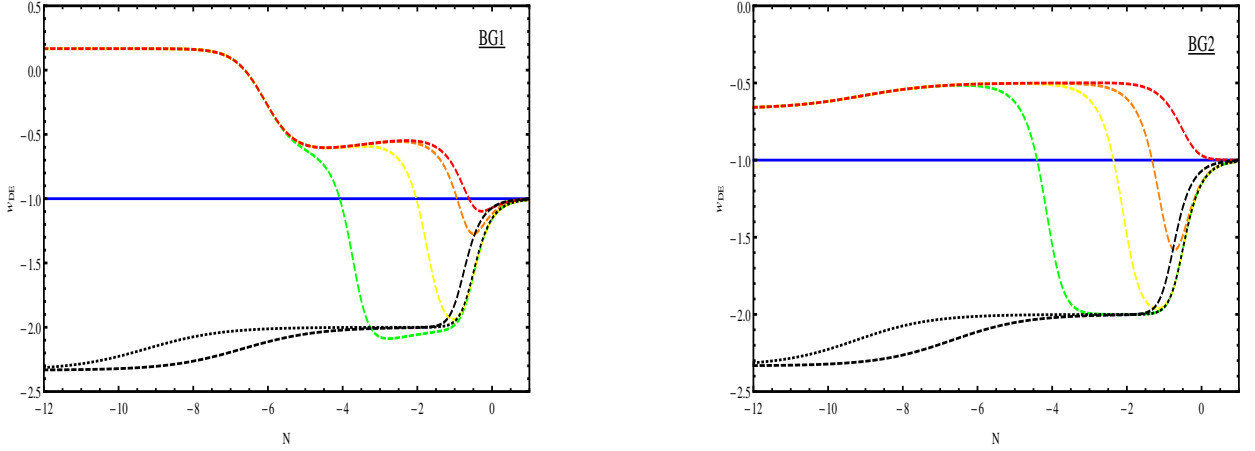


FIG. 2. Evolution of dark energy equation of state w_{DE} for BG1 and BG2 models. The initial conditions for BG1 models are: $r_1^{(s)} = 10^{-14}$, $r_2^{(s)} = 2 \times 10^{-23}$ and $r_3^{(s)} = 10^3$ (Green), $r_3^{(s)} = 10^5$ (Yellow), $r_3^{(s)} = 2 \times 10^6$ (Orange), $r_3^{(s)} = 5 \times 10^6$ (Red). The initial conditions for BG2 model are: $r_1^{(s)} = 10.0522$, $r_2^{(s)} = 2 \times 10^{-63}$ and $r_3^{(s)} = 10^{17}$ (Green), $r_3^{(s)} = 10^{19}$ (Yellow), $r_3^{(s)} = 2 \times 10^{20}$ (Orange), $r_3^{(s)} = 5 \times 10^{20}$ (Red). The tracker solutions **T1** and **T2** are shown by the black dashed and dotted curves, respectively.

V. GROWTH RATE OF MATTER PERTURBATIONS

The study of the growth rate of cosmological density perturbations has become a powerful tool to distinguish between cosmological models based on modified theories of gravity and dark energy models. Even all models can perfectly mimic the Λ CDM evolution at the background level, they all intrinsically alter the structure formation. An important probe in this context is the evolution of linear matter density contrast $\delta_m \equiv \delta\rho_m/\rho_m$ which verify the following equation

$$\ddot{\delta} + 2H\dot{\delta} - 4\pi G_{eff}\rho_m \approx 0 \quad (69)$$

where G_{eff} is a function of the scale factor and the cosmological scale. The matter density contrast is related to the observed quantity $f(a)\sigma_8(a)$ where $f(a) = d\ln\delta(a)/d\ln(a)$ and $\sigma_8(a) = \sigma_8\delta_m(a)/\delta_m(1)$ is the rms fluctuations of the linear density field inside a radius of $8h^{-1}$ Mpc, and σ_8 is its present value.

We propose now to study the evolution of the equations (2), (3) and (4) at the perturbed level. We consider only

scalar perturbations of the flat FRW metric in the Newtonian gauge

$$ds^2 = (1 - 2\Phi)dt^2 - a(t)^2(1 + 2\Psi)\delta_{ij}dx^jdx^i, \quad (70)$$

where Φ and Ψ are scalar metric perturbations related to the Newtonian potential and perturbation of the spatial three-curvature. Perturbing the scalar fields and the matter density, $\varphi^I \rightarrow \varphi^I(t) + \delta\varphi^I(t, x^i)$, $\rho_m \rightarrow \rho_m(1 + \delta(t, x^i))$ and keeping perturbations at first order, the Einstein equations (2) thus take the form

(0, 0):

$$\begin{aligned} & \frac{k^2}{a^2} \left(\Psi - \frac{1}{2}b_{IJK}\dot{\varphi}^J\dot{\varphi}^K\delta\varphi^I \right) - \frac{1}{4}a_{IJ}\delta[\dot{\varphi}^J\dot{\varphi}^I] + 9Hb_{IJK}\dot{\varphi}^I\dot{\varphi}^J\delta\dot{\varphi}^K \\ & + 3 \left(H - \frac{1}{2}b_{IJK}\dot{\varphi}^I\dot{\varphi}^J\dot{\varphi}^K \right) \dot{\Psi} - (3Hb_{IJK}\dot{\varphi}^I\dot{\varphi}^J\dot{\varphi}^K + 2\rho_m) \Phi = \rho_m\delta, \end{aligned} \quad (71)$$

(i, i):

$$\begin{aligned} & -\frac{k^2}{a^2}(\Psi - \Phi) - 3(\ddot{\Psi} + 3H\dot{\Psi}) - \frac{3}{4}a_{IJ}\delta(\dot{\varphi}^J\dot{\varphi}^I) - 3b_{IJK}\dot{\varphi}^I\dot{\varphi}^J\delta\dot{\varphi}^K - \frac{3}{2}b_{IJK}\dot{\varphi}^J\dot{\varphi}^I\delta\ddot{\varphi}^K \\ & - 3 \left(H + \frac{1}{2}b_{IJK}\dot{\varphi}^J\dot{\varphi}^I\dot{\varphi}^K \right) \dot{\Phi} - \frac{3}{2} \left(6\dot{H} + 4H^2 + a_{IJ}\dot{\varphi}^J\dot{\varphi}^I + 2b_{IJK}\dot{\varphi}^I\dot{\varphi}^J\ddot{\varphi}^K \right) (\Phi + \Psi) = 0, \end{aligned} \quad (72)$$

(i, 0):

$$-\dot{\Psi} - \frac{1}{2}b_{IJK}\dot{\varphi}^I\dot{\varphi}^J\delta\dot{\varphi}^K - \left(\frac{1}{2}a_{IJ}\dot{\varphi}^J - \frac{3}{2}b_{IJK}\dot{\varphi}^J\dot{\varphi}^K \right) \delta\varphi^I - (H + b_{IJK}\dot{\varphi}^I\dot{\varphi}^J\dot{\varphi}^K) \Phi = \rho_mv, \quad (73)$$

(i ≠ j):

$$\partial_i\partial_j(\Psi - \Phi) = 0, \quad (74)$$

where k is the cosmological scale.

The BG field equations (5), up to linear order in perturbations, are given by

$$\begin{aligned} & (a_{IJ} + 6b_{IJK}H\dot{\varphi}^K) \delta\ddot{\varphi}^J + 3 \left(a_{IJ}H + 2b_{IJK}(H\ddot{\varphi}^K + 3H^2\dot{\varphi}^K + \dot{H}\dot{\varphi}^K) \right) \delta\dot{\varphi}^J \\ & + \frac{k^2}{a^2} (a_{IJ} - 2b_{IJK}(2H\dot{\varphi}^K + \ddot{\varphi}^K)) \delta\varphi^J \\ & + 3b_{IJK}\dot{\varphi}^J\dot{\varphi}^K\ddot{\Phi} - \left(2a_{IJ}\dot{\varphi}^J + 9Hb_{IJK}\dot{\varphi}^J\dot{\varphi}^K + 6b_{IJK}\dot{\varphi}^J\ddot{\varphi}^K\dot{\Phi} \right) \dot{\Phi} \\ & - 2 \left(a_{IJ}H\dot{\varphi}^J + 4b_{IJK}H\dot{\varphi}^J\ddot{\varphi}^K + 6b_{IJK}\dot{H}\dot{\varphi}^J\dot{\varphi}^K + 18H^2b_{IJK}\dot{\varphi}^J\dot{\varphi}^K - \frac{k^2}{2a^2}b_{IJK}\dot{\varphi}^J\dot{\varphi}^K \right) \Phi = 0. \end{aligned} \quad (75)$$

In deriving Eq. (75) we have used the background equation of motion (13) and $\Psi = \Phi$ from (74). Similarly, the perturbed equations of motion for pressurless matter field (4) are given by

$$\delta\dot{\rho}_m + 3H\delta\rho_m = \left(\frac{k}{a^2} \right) \rho_mv - 3\rho_m\dot{\Phi}, \quad (76)$$

$$\dot{v} = \Phi \quad (77)$$

where v is the potential of velocity matter perturbation.

Defining the gauge-invariant matter density contrast

$$\delta_m := \delta\rho_m - 3Hv \quad (78)$$

we write the matter field perturbation in Fourier space as

$$\ddot{\delta}_m + 2H\dot{\delta}_m + \frac{k^2}{a^2}\delta_m = 3 \left(\ddot{Q} + 2H\dot{Q} \right) \quad (79)$$

where $Q = Hv - \Phi$. Since matter perturbations evolve on spatial scales much smaller than of the Hubble horizon ($k \gg aH$), we use the so called quasi-static approximation on sub-horizon scales. Under this approximation, the

dominant terms in the perturbed equations are those including δ_m and k^2/a^2 . Then, Eqs. (74), (71), (79) and (75) in the sub-horizon approximation read

$$\frac{k^2}{a^2} \left(\Phi - \frac{1}{2} b_{IJK} \dot{\varphi}^J \dot{\varphi}^K \delta\varphi^I \right) + \rho_m \delta_m = 0 \quad (80)$$

$$b_{IJK} \dot{\varphi}^J \dot{\varphi}^K \Phi + (a_{IJ} - 2b_{IJK} (2H\dot{\varphi}^K + \ddot{\varphi}^K)) \delta\varphi^J = 0 \quad (81)$$

$$\ddot{\delta}_m + 2H\dot{\delta}_m + \frac{k^2}{a^2} \Phi = 0 \quad (82)$$

These equations can be solved for Φ , $\delta\varphi^1$ and $\delta\varphi^2$, and as a result we obtain

$$-\frac{k^2}{a^2} \Phi = \frac{\text{Det} [\mathbf{K}]}{\text{Det} [\mathbf{M}]} \rho_m \delta_m, \quad (83)$$

$$-\frac{k^2}{a^2} \delta\varphi^I = \frac{L_2 K_{1I} - L_1 K_{2I}}{\text{Det} [\mathbf{M}]} \rho_m \delta_m, \quad (84)$$

where the matrices \mathbf{M} and \mathbf{K} , and the vector \mathbf{L} are given by

$$\mathbf{M} = \begin{pmatrix} 1 & \frac{1}{2} \mathbf{L}^T \\ \mathbf{L} & \mathbf{K} \end{pmatrix}, \quad (85)$$

$$K_{IJ} = (a_{IJ} - 2b_{IJK} (2H\dot{\varphi}^K + \ddot{\varphi}^K)), \quad (86)$$

$$L_I = b_{IJK} \dot{\varphi}^J \dot{\varphi}^K. \quad (87)$$

Equation (83) is the modified Poisson equation, $-\frac{k^2}{a^2} \Phi = G_{eff} \rho_m \delta_m$, where the effective gravitational coupling is given by

$$G_{eff} = \frac{\text{Det} [\mathbf{K}]}{\text{Det} [\mathbf{M}]} G_N, \quad (88)$$

where we have restored Newton's constant G_N . As we see, the effective gravitational coupling is a function of $\dot{\varphi}^K$ and $\ddot{\varphi}^K$, and is therefore subject to change. In terms of the dynamical variables (27) G_{eff} is expressed as

$$\begin{aligned} \frac{G_{eff}}{G_N} = \frac{8}{D} & \left(-(\alpha + 2)^2 r_3^2 (\epsilon_{\varphi_2} + 2)^2 - (\epsilon_{\varphi_1} + 2) ((\alpha - 2)^2 \epsilon_{\varphi_1} + 4((\alpha - 2)\alpha + 2)) \right. \\ & \left. + \alpha(\alpha + 2)r_3 (3\epsilon_{\varphi_1} + (2\epsilon_{\varphi_1} + 5)\epsilon_{\varphi_2} + 8) + 6r_1 \left(-(3\alpha - 2)(\epsilon_{\varphi_1} + 2) + \alpha r_3 (2\epsilon_{\varphi_2} + 5) \right) \right) \end{aligned} \quad (89)$$

where

$$\begin{aligned} D = & r_2 \left((\alpha + 2)^3 r_3^4 (\epsilon_{\varphi_1} - 4\epsilon_{\varphi_2} - 6) - (3\alpha - 2) (4(\alpha^2 - 2\alpha + 2) + (\alpha - 2)^2 \epsilon_{\varphi_1}) \right. \\ & + 2\alpha(\alpha + 2)^2 r_3^3 (6\epsilon_{\varphi_2} + 11) + 2\alpha r_3 (12 - 12\alpha + 17\alpha^2 + 4(\alpha - 2)^2 \epsilon_{\varphi_1} \\ & + 2(\alpha^2 + 4\alpha - 4)\epsilon_{\varphi_2}) - 2\alpha + 2r_3^2 (8 - 8\alpha + 19\alpha^2 + 3(\alpha - 2)^2 \epsilon_{\varphi_1} - (8 \\ & 6\alpha^2 + 8\alpha)\epsilon_{\varphi_2})) + 8((\epsilon_{\varphi_1} + 2) (4(\alpha^2 - 2\alpha + 2) + (\alpha - 2)^2 \epsilon_{\varphi_1}) + (2 \\ & \alpha)^2 r_3^2 (\epsilon_{\varphi_2} + 2)^2 - \alpha(\alpha + 2)r_3 (5\epsilon_{\varphi_2} + \epsilon_{\varphi_1} (2\epsilon_{\varphi_2} + 3) + 8)) - 6r_1 (r_2 (-1 \\ & + r_3)^2 (-3\alpha + (\alpha + 2)r_3 + 2)^2 8(\alpha r_3 (2\epsilon_{\varphi_2} + 5) - (3\alpha - 2)(\epsilon_{\varphi_1} + 2))) \end{aligned} \quad (90)$$

where ϵ_{φ_1} , ϵ_{φ_2} are given by (34) and (35). Along the trackers the effective gravitational coupling simplifies to

$$\frac{G_{eff}}{G_N} = \frac{2 \left(\Omega_{DE}^{(i)} - 2 \right) + \Omega_r}{4 - \Omega_{DE}^{(i)} \left(\Omega_{DE}^{(i)} + 3 \right) + \Omega_r} \quad (91)$$

where $\Omega_{DE}^{(i)}$ is given by (59). In radiation and matter epochs, where $\Omega_{DE}^{(i)} \ll 1$, we have $G_{eff} \rightarrow 1$, while In dS epoch where $\Omega_{DE}^{(i)} \approx 1$, we get $G_{eff} \rightarrow \infty$ for both tracker solutions as in [28].

In the small regime the effective gravitational coupling is approximated by the relation

$$G_{eff} \approx 1 - \frac{3(\alpha - 2)}{2(\Omega_r + 5)} r_3^2 r_2, \quad (92)$$

while in the regime where r_3 dominates over r_1 and r_2 and using $r_1 = (2 - \alpha)/2$, G_{eff} takes the form

$$G_{eff} \approx G_N \left[1 - \frac{3(\alpha - 2)(\Omega_r + 9)}{2(\Omega_r + 5)^2} r_3^2 r_2 \right]. \quad (93)$$

It follows that in the range $\alpha < -1$, the gravitational interaction is stronger than that in General Relativity.

VI. OBSERVATIONAL CONSTRAINTS

In this section, we place observational bounds on the BG model by performing a Markov Chain Monte Carlo (MCMC) integration via the Metropolis-Hasting algorithm. To get tighter constraints we use recent compilation of the redshift space distortion (RSD) datasets (for our purpose we only consider the bottom 20 data in Table. III) [42, 43], combined with the model-independent observational Hubble (OHD) dataset obtained through the differential age method [44] shown in Table. IV. The resulting combined Likelihood function reads

$$\mathcal{L}(\hat{\theta}) = \mathcal{L}_{RSD} \times \mathcal{L}_{OHD} \quad (94)$$

and $\hat{\theta}$ is the vector of model parameters over which the MCMC integration is performed. We consider two cases of the space parameters for the BG model. In the first case labeled as BG1 model the space parameter is given by the vector $\hat{\theta} = (\alpha, r_{1i}, r_{2i}, r_{3i}, \Omega_{m0}, \sigma_8)$ and the second case which follows from the dark energy solution found in IV C is labeled as BG2 model. The later and is described by the space parameter given by $\hat{\theta} = (\alpha, r_{2i}, r_{3i}, \Omega_{m0}, \sigma_8)$, where the initial condition on r_1 is fixed as $r_1^{(s)} = (2 - \alpha)/2$. The BG2 model has one parameter less than the BG1 model and it is expected that it will be less penalized than the BG1 model by Bayesian selection. Without using any fiducial cosmology to correct the $f\sigma_8$ measurements, we confront our findings with the 68%, 95% and 99% confidence limits of Λ CDM and w CDM models.

A. Constrained parameter space

The best fits results of the parameters $r_1^{(s)}, r_2^{(s)}, r_3^{(s)}, \alpha, \Omega_m, h, w$ and σ_8 with 68% Confidence Level (CL) limits for the BG1, BG2, Λ CDM and w CDM models are summarized in Table. II. The constrained parameters are compatible with that of Λ CDM and w CDM models, and are consistent with Planck collaboration data [3, 4]. We note also the similarity between the BG1 and BG2 models. But taking into account that the BG2 model has one less parameter than the BG1 model, the BG2 it is slightly favored.

In Fig. 3 we have shown the best fits evolution of the dark energy equation of state w_{DE} for BG1 and BG2 models. As already noted above, w_{DE} follow two different paths in the radiation epoch until they merge in one path in the matter epoch. The evolution of w_{DE} in BG2 model is better than that of BG1 model since it is close to the Λ CDM model and is in the region $-0.5 < w_{DE} < -1.044$ during all cosmological epochs.

In Fig. 4 we have plotted the evolution of Hubble parameter for the BG2 model and compared it with the Λ CDM model and the OHD data. We observe that the curves are indistinguishable at low redshifts, but they start to differ slightly at high redshifts.

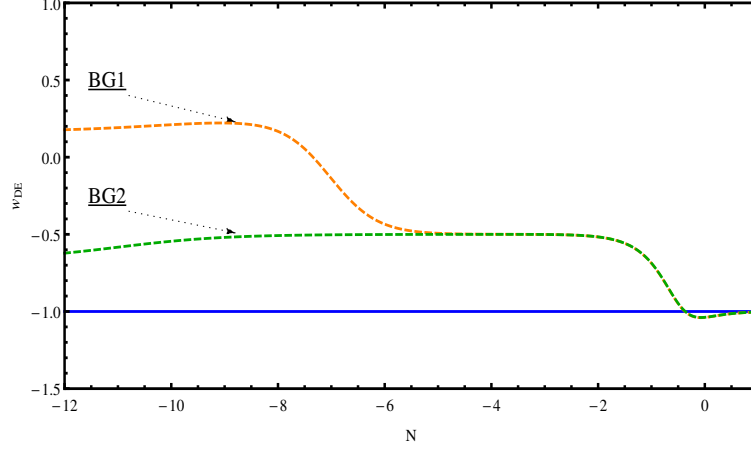


FIG. 3. Plot of the best fits evolution of the dark energy equation of state w_{De} for BG1 and BG2 models with respect to $N = \ln a$. The best fit parameters used for this plot are given in Table.II.

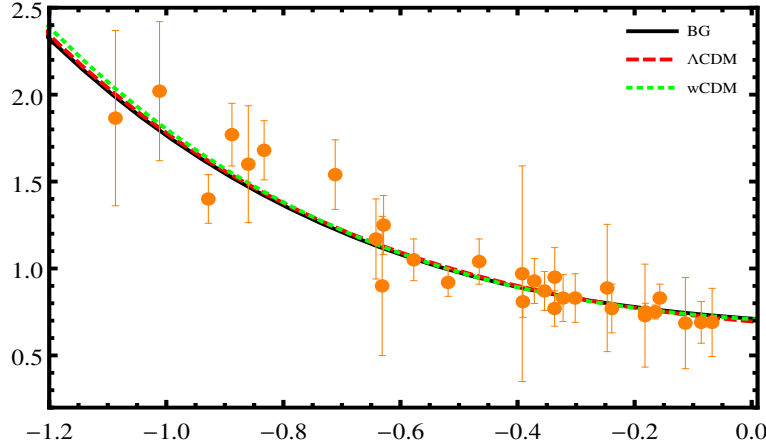


FIG. 4. Plot of the best fits evolution of the Hubble parameter for the BG2, Λ CDM and w CDM models with respect to $N = \ln a$. We have also plotted the Hubble data with 1σ errors from the OHD data compilation [44].

We also plotted the observationally allowed regions with 1σ , 2σ and 3σ CL limits for parameters α , Ω_m , h , w and σ_8 for the BG2, Λ CDM and w CDM models. In Fig. 5, the combined recent RSD and OHD datasets lead the best fit values with 1σ error for σ_8 and $\Omega_m^{(0)}$ as $(0.7968^{+0.0148}_{-0.0148}, 0.2586^{+0.0277}_{-0.0277})$ for the BG model, and are at 1.5σ from Planck15 values. The best fit values found for the Λ CDM, $(0.8104^{+0.0407}_{-0.0407}, 0.2926^{+0.0319}_{-0.0319})$, are in agreement within 1σ with Planck15 values. Recently, σ_8 and $\Omega_m^{(0)}$ for a Λ CDM cosmology, have been constrained by tomographic weak gravitational lensing data in KiDS-450 survey [45], and by galaxy clustering and weak gravitational lensing data from the first year of the Dark Energy Survey (DES) [46] through the relation $S_8 = \sigma_8 \sqrt{\Omega_m^{(0)}/0.3}$. In KiDS-450 survey they found $S_8 = 0.745 \pm 0.039$, which is at 2.3σ from Planck results, while in DES survey the best fit value, $S_8 = 0.783^{+0.021}_{-0.025}$, is within 1σ region of Planck results. In order to adapt the predictions from these datasets for the BG model we follow [47]. The value of S_8 at a given red-shift for the Λ CDM cosmology is given by

$$\begin{aligned}
 S_{8(\Lambda)}(\bar{z}) &= \sigma_{8(\Lambda)} g_{(\Lambda)}(\bar{z}) \sqrt{\frac{\Omega_{m(\Lambda)}(\bar{z})}{0.3}} \\
 &= S_{8(\Lambda)} g_{(\Lambda)}(\bar{z}) \sqrt{\frac{\Omega_{m(\Lambda)}(\bar{z})}{\Omega_{m(\Lambda)}^{(0)}}},
 \end{aligned} \tag{95}$$

where \bar{z} is some averaged redshift, $g(z) = \delta(z)/\delta(0)$ of the growth function, and the subscript (Λ) stands for Λ CDM quantities.

For the BG model we use the rescaled relations [47]

$$S_8 = S_{8(\Lambda)} \frac{g_{(\Lambda)}(\bar{z})}{g(\bar{z})} \sqrt{\frac{\Omega_{m(\Lambda)}(\bar{z})}{\Omega_m(z)}} \sqrt{\frac{\Omega_m^{(0)}}{\Omega_{m(\Lambda)}^{(0)}}}, \quad (96)$$

$$\sigma_8 = \sigma_{8(\Lambda)} \frac{g_{(\Lambda)}(\bar{z})}{g(\bar{z})} \sqrt{\frac{\Omega_{m(\Lambda)}(\bar{z})}{\Omega_m(z)}}. \quad (97)$$

Considering an average value $\bar{N} = -0.4055$ ($\bar{z} = 0.5$), we get the following best fit values

$$\begin{aligned} S_8 &= 0.734 \pm 0.081, \sigma_8 = 0.791 \pm 0.086 \quad \text{for KiDS-450 survey,} \\ S_8 &= 0.771 \pm 0.078, \sigma_8 = 0.831 \pm 0.082 \quad \text{for DES survey.} \end{aligned}$$

In the case of KiDS-450 data, the best fit value for σ_8 is in agreement with the value we have obtained using RSD+H(z) measurements, and still compatible with Planck values. On the other the σ_8 value in the context of DES survey does not agree with the best fit value we found with RSD+H(z) measurements, but it is within the 1σ region of Planck results. We conclude that the best fit BG2 model is in concordance with both data, but it is slightly favored if we used instead the DES survey data.

Finally, considering the w CDM model we found the best fit values, $\sigma_8 = 0.7858^{+0.0597}_{-0.0597}$ and $\Omega_m^{(0)} = 0.2987^{+0.0402}_{-0.0402}$ which are also close to the 1σ region of Planck values. Our best fit values are at 1.5σ , 0.81σ and 1.1σ from Planck, Λ CDM, and w CDM best fit values, respectively. Therefore, we conclude that the BG2 provides a rate of structure clustering in agreement with current observations.

In Fig. 6, the combined data RSD+H(z) lead to higher values of h at 1σ ($h = 0.7116^{+0.0288}_{-0.0288}$), in the range of the values found in [8, 9, 48]. This value is very close to the recent local measurement of Hubble constant, $H_0 = 69.8 \pm 0.8$ [49], and therefore eases the persistent tension on the Hubble constant. In Fig. 7, we show the data constraints on the today dark energy equation of state w_0 . The best fit value for the BG2 model, $w_0 = -1.0377^{+0.068}_{-0.068}$ is very close to -1 , and that the BG2 model is more constrained by the data than the w CDM model regarding the constraints from Planck15/ w CDM.

In Fig. 8, the probability contours in the (Ω_m, α) and (σ_8, α) -planes show that the coupling constant is constrained by the data to $\alpha = -18.1045^{+3.366}_{-3.366}$.

Fig. 9 shows the best fit behavior of $f\sigma_8(N)$ for the BG1 and BG2 models. The two models are indistinguishable, and we notice that the strenght of fluctuations is stronger than that of the Λ CDM and w CDM models starting from redshift $z \approx 0.41, 0.35$ to the present epoch, respectively. This means that the structures cluster faster in the BG model than in the Λ CDM and w CDM models in this recent past epoch, and this effect is due to increasing behavior of the effective gravitational constant. Compared to Planck15 data, the strength of the fluctuations in the BG models becomes stronger only starting from $z \gtrsim 0.004$. Even we have only considered in our study the RSD data published recently, it is this particular behavior of matter fluctuations in the BG model which make our results are still consistent with the full growth data. Finally, we provide a parametrization for $f\sigma_8(z)$ in the BG2 model assuming the Λ CDM background in the form $f\sigma_8(z) = \rho\sigma_8\Omega_m(z)^\gamma / (1+z)^\beta$. Using Planck15 data we obtain an excellent fit to the numerical solution of Eqs.(69) and (89) with the best fit parameters $\rho \approx 1.16$, $\gamma \approx 0.6$ and $\beta \approx 0.93$. These values are very close to that obtained in modified gravity theory parametrization of $G_{eff}(z)$ [42, 43].

Parameter	BG1	BG2	Λ CDM	w CDM
	$\chi^2_{min} = 21.8994$	$\chi^2_{min} = 21.8795$	$\chi^2_{min} = 19.8405$	$\chi^2_{min} = 19.83$
α	-18.1 ± 3.4658	-18.1045 ± 3.3660	—	—
$r_{1i} (.10^{-14})$	26.8058 ± 5.3154	—	—	—
$r_{2i} (.10^{-22})$	6.45 ± 2.42323	$(6.734 \pm 2.4047) \times 10^{-40}$	—	—
$r_{3i} (.10^6)$	8.2042 ± 2.7431	$(2.5 \pm 0.9306) \times 10^{14}$	—	—
$\Omega_m^{(0)} h^2$	0.1305 ± 0.01	0.1309 ± 0.009	0.1406 ± 0.0136	0.15 ± 0.0219
σ_8	0.7919 ± 0.0177	0.7968 ± 0.0148	0.8104 ± 0.0407	0.7858 ± 0.0597
h	0.7111 ± 0.0298	0.7116 ± 0.0288	0.6953 ± 0.0246	0.7088 ± 0.0519
w_0	-1.0385 ± 0.0756	-1.0377 ± 0.0682	—1	-1.1421 ± 0.3465
$\Omega_m^{(0)}$	0.2581 ± 0.028	0.2586 ± 0.0277	0.2926 ± 0.0319	0.2987 ± 0.0402
$\ln B_{ij}/\Lambda$ CDM	—0.5	—0.25	—	—0.33
$\ln B_{ij}/w$ CDM	—0.16	0.08	0.33	—

TABLE II. 1σ Parameter confidence level for the BG, Λ CDM and w CDM models from late RSD dataset combined with OHD dataset. The parameters h and w are derived parameters for the BG models, while Ω_{m0} is a derived parameter for all the models. The negative values of $\ln B_{ij}$ imply that Λ CDM and w CDM models are preferred over the BG1 and BG2 models.

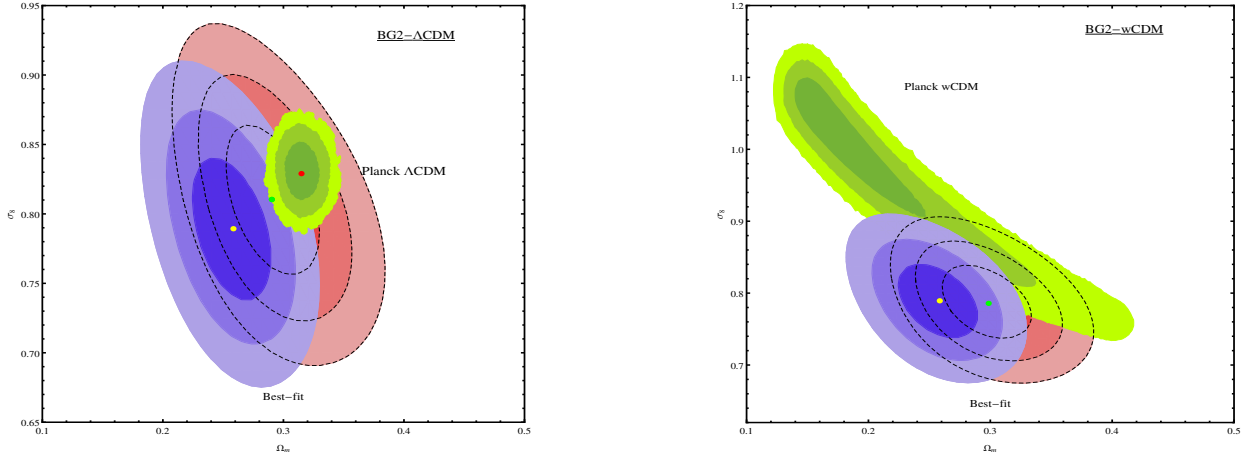


FIG. 5. Probability contours in the (Ω_m, σ_8) -plane for BG2, Λ CDM and w CDM models from combined RSD data and OHD data. The filled dark, medium and light colored contours enclose 68.3, 95.4 and 99.7% of the probability, for BG2 model (blue) and CDM models (Red), respectively. The light Green contours correspond the Planck15/ Λ CDM[3].

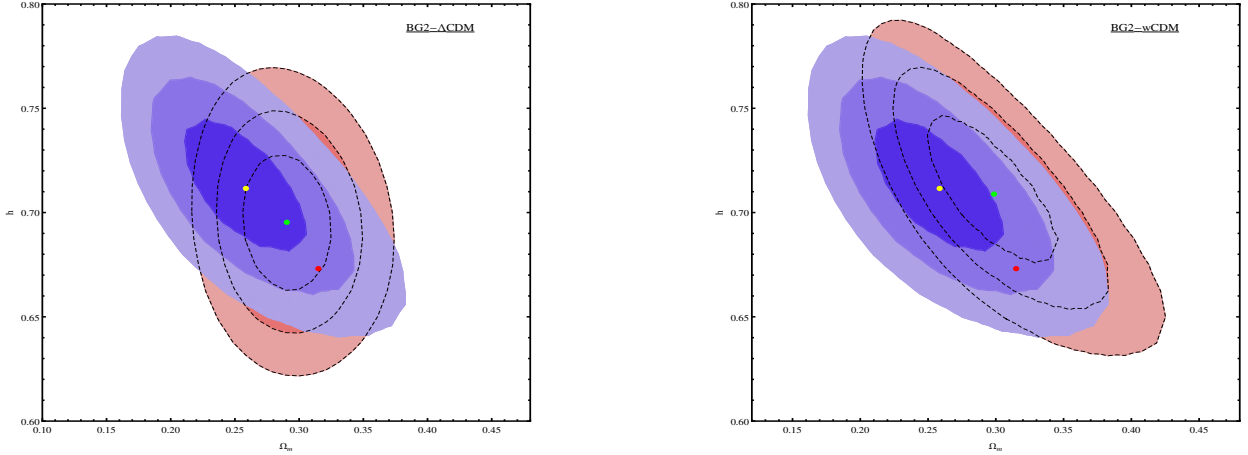


FIG. 6. Probability contours in the (Ω_m, h) -planes for BG2, Λ CDM and w CDM models from combined RSD data and OHD data. The filled dark, medium and light colored contours enclose 68.3, 95.4 and 99.7% of the probability, for BG2 model (blue) and CDM models (Red), respectively. The light Green contours correspond the Planck15/ Λ CDM[3].

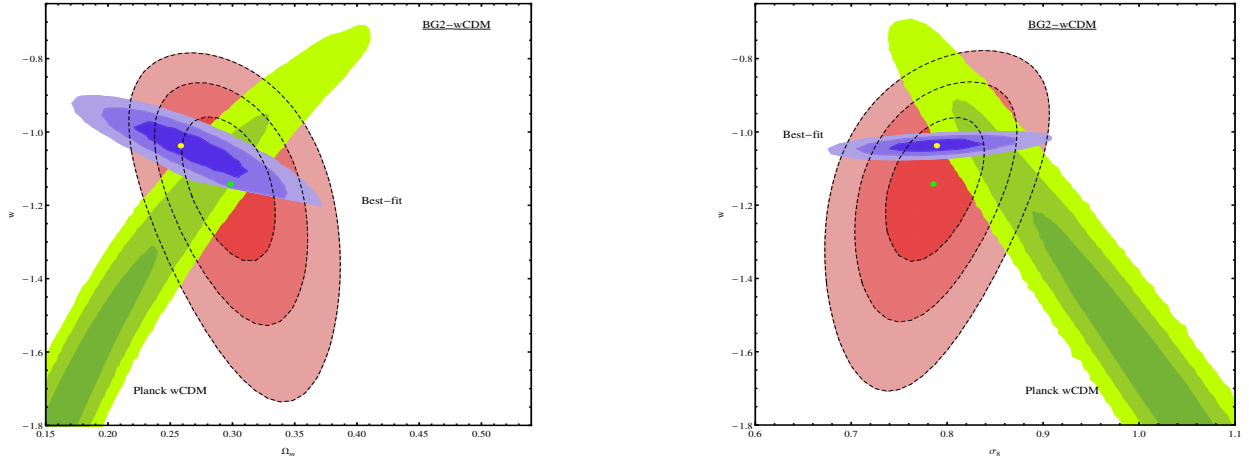


FIG. 7. Probability contours in the (Ω_m, w) and (σ_8, w) -planes for BG2 and wCDM models from combined RSD data and OHD data. The filled dark, medium and light colored contours enclose 68.3, 95.4 and 99.7% of the probability, for BG2 model (blue) and wCDM model (Red), respectively. The light Green contours correspond the Planck15/wCDM[3].

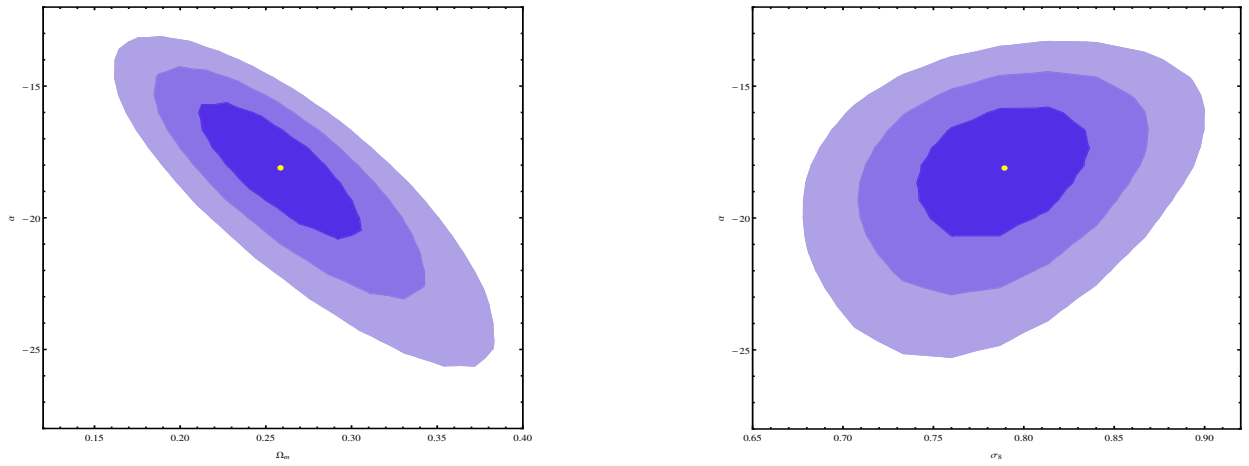


FIG. 8. Probability contours in the (Ω_m, α) , (σ_8, α) -planes for BG2 model from combined RSD data and OHD data. The filled dark, medium and light blue contours enclose 68.3, 95.4 and 99.7% of the probability, respectively.

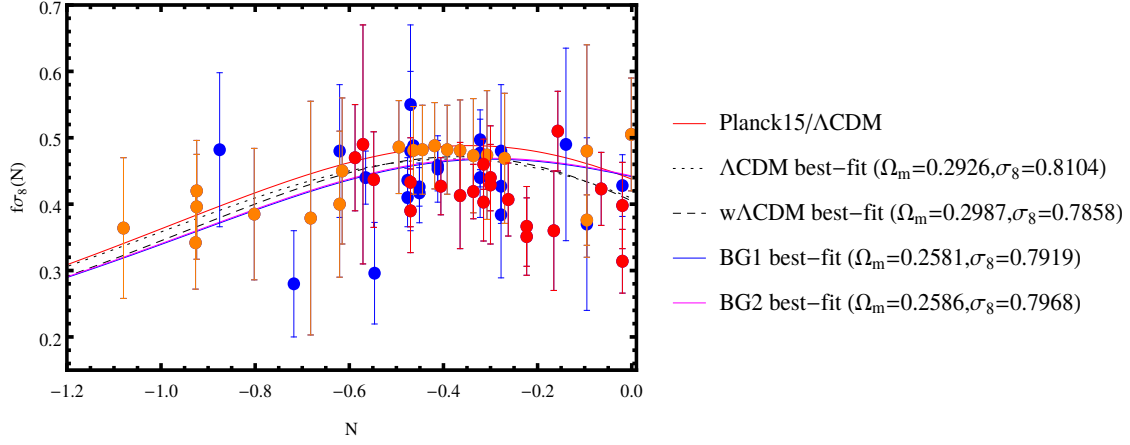


FIG. 9. Plot of $f\sigma_8(N)$ as a function of the number of e-folds for the 20 latest growth rate data set (Orange). We also show the earliest data points (Red) and the remaining published data points (Blue) taken from Table III. The red curve corresponds to Planck15/ Λ CDM best fits. The indistinguishable blue and cyan solid lines corresponds to the best fits BG1 and BG2 models respectively, whereas the dotted and dashed black lines corresponds to the best fits Λ CDM and w CDM models, respectively.

B. Bayesian analysis

In order to see whether the BG models are favored over the Λ CDM and w CDM models, we use Bayesian analysis where the central quantity is the posterior probability of the parameter space θ subjected to observational data and prior information. Given two models \mathcal{M}_A and \mathcal{M}_B the posterior beliefs on the two models is given by

$$\frac{\Pr(\mathcal{M}_A | \mathcal{Y})}{\Pr(\mathcal{M}_B | \mathcal{Y})} = \frac{\pi(\mathcal{M}_A) \Pr(\mathcal{Y} | \mathcal{M}_A)}{\pi(\mathcal{M}_B) \Pr(\mathcal{Y} | \mathcal{M}_B)} \quad (98)$$

where $\pi(\mathcal{M}_i)$ is the prior belief on the model \mathcal{M}_i . The updating term on the RHS of Eq.(98), $B_{AB} = \Pr(\mathcal{Y} | \mathcal{M}_A) / \Pr(\mathcal{Y} | \mathcal{M}_B)$, is Bayes factor of the model \mathcal{M}_A relative to the reference model \mathcal{M}_B , and is a key quantity in Bayesian hypothesis testing [50]. The Bayes factor provides a direct measure of the weight of evidence provided by data for the reference model. A quantification of this measure is provided by the classification proposed by Kass and Raftery [50], where $1 < B_{ij} < 3$ is interpreted as weak evidence; $3 < B_{ij} < 20$ as positive evidence; $20 < B_{ij} < 150$ as strong evidence; and $B_{ij} > 150$ as very strong evidence in favor of the reference model.

We have calculated the Bayes factor taking the Λ CDM and w CDM models as the reference models. In the first case the datasets exhibit the preference of the Λ CDM with only three free parameters over the BG1, BG2 and w CDM models. On the other hand the BG2 model with one extra parameter than in w CDM model is slightly preferred with a score 0.08 of Bayes factor.

VII. CONCLUSIONS

In this paper, we studied the background cosmology and the evolution of matter density perturbations in a covariant multi-Galileons field model. In particular, we considered the cubic bi-Galileon (BG) model with two scalar fields φ^1 and φ^2 and constant coupling functions. We showed that the BG model exhibits a rich dark energy structure compared to the single Galileon (SG) model. The phase space analysis of the dynamical equations of the background cosmology allowed us to identify a set of fixed points and their properties in each cosmological epoch, and that the supplementary dynamical variable $r_3 = \dot{\varphi}^2 / \dot{\varphi}^1$, compared to the SG field model, plays a crucial role in the cosmological dynamics of the BG model. We found that the BG model possess two tracker solutions, one is the usual tracker solution of the SG field model and the other is considered as the signature of the second field. We investigate the properties of the BG model by considering two cases, the first one, labeled BG1, consists in analyzing the full set of equations of the dynamical system, and the second case, labeled BG2, is based on the dark energy solution found in Sec. IV C valid in the regime where $r_3^{(s)} \gg \{1, r_1^{(s)}\}$ and $r_2^{(s)} \ll 1$ to guaranty $\Omega_{DE} \ll 1$ radiation and matter epochs. We show that the cosmological evolution prefer the path of the second, tracker at earlier or later

times depending on the initial conditions. However, these tracker solutions are disfavored by observational data due to the bad behavior of the dark energy equation of state in matter epoch ($w_{DE} = -2$), exactly like the cubic SG model. However, in the regime of initial conditions $r_3^{(s)} \gg \{1, r_1^{(s)}\}$ and $r_2^{(s)} \ll 1$, we found that the approach to the tracker is prevented in BG1 and BG2 models, respectively. In fact, we showed that the dark energy solution in this regime with the initial condition $r_1^{(s)} = (2 - \alpha)/2$, gives the best sequence of the evolution of the dark energy equation of state, $w_{DE} = -2/3$ (radiation era) $\rightarrow -1/2$ (matter era) $\rightarrow -1$ (dS era). We studied also the growth rate of matter perturbation in the quasi-static approximation on sub-horizon scales, and obtained the evolution equation of the matter density contrast with an effective gravitational coupling showing that gravity is stronger than that in General Relativity. Using the combination of the latest RSD data and the OHD data compilations, we put observational constraints on free parameters in the BG model by running the MCMC simulation using Hasting-Metropolis algorithm assuming flat priors for the fitting parameters. We considered the two models BG1 and BG2 with six and five parameters, respectively. The results obtained from the likelihood analysis shows that both the BG models give practically indistinguishable best fits parameters ($\alpha, \Omega_m, w, h, \sigma_8$) where α is the coupling function, and are compatible with the Planck15 (TT+lowE) observations data. Indeed the best fits value of σ_8 for the BG2 model, $\sigma_8 = 0.7968 \pm 0.0148$, is very close to Planck15 1σ uncertainties. More interestingly, we have found that the best fits values of the Hubble constant, $h = 0.7116 \pm 0.0288$, can ease the persistent tension between CMB [4] and Cepheid distance scale measurements at low redshifts [9]. Finally, according to model selection using the Bayes factor, we found that the BG2 model is disfavored compared to Λ CDM model but slightly preferred over the w CDM model. In future works, it will be of interest to place stronger constraints on the initial conditions $r_i^{(s)}$ and cosmological parameters using other observational data such Type Ia Supernovae (SnIa), Baryon Acoustic Oscillation (BAO), Weak Lensing (WL) and Cosmic Microwave Background (CMB) measurements.

ACKNOWLEDGMENTS

The research of K. N was supported by the The Algerian Ministry of Higher Education and Scientific Research grant no. "cnepru-d01720140008".

Appendix: Tables of data

TABLE III. Redshift Space Distorsion data compilation [42, 43].

Index	Data set	z	$f\sigma_8(z)$	References
1	SDSS-LRG	0.35	0.440 ± 0.050	[51]
2	VVDS	0.77	0.490 ± 0.18	[51]
3	2dFGRS	0.17	0.510 ± 0.060	[51]
4	2MRS	0.02	0.314 ± 0.048	[52, 53]
5	SnIa+IRAS	0.02	0.398 ± 0.065	[53, 54]
6	SDSS-LRG-200	0.25	0.3512 ± 0.0583	[55]
7	SDSS-LRG-200	0.37	0.4602 ± 0.0378	[55]
8	SDSS-LRG-60	0.25	0.3665 ± 0.0601	[55]
9	SDSS-LRG-60	0.37	0.4031 ± 0.0586	[55]
10	WiggleZ	0.44	0.413 ± 0.080	[56]
11	WiggleZ	0.60	0.390 ± 0.063	[56]
12	WiggleZ	0.73	0.437 ± 0.072	[56]
13	6dFGS	0.067	0.423 ± 0.055	[57]
14	SDSS-BOSS	0.30	0.407 ± 0.055	[58]
15	SDSS-BOSS	0.40	0.419 ± 0.041	[58]
16	SDSS-BOSS	0.50	0.427 ± 0.043	[58]
17	SDSS-BOSS	0.60	0.433 ± 0.067	[58]
18	Vipers	0.80	0.470 ± 0.080	[59]
19	SDSS-DR7-LRG	0.35	0.429 ± 0.089	[60]
20	GAMA	0.18	0.360 ± 0.090	[61]
21	GAMA	0.38	0.440 ± 0.060	[61]
22	BOSS-LOWZ	0.32	0.384 ± 0.095	[62]
23	SDSS DR10 and DR11	0.32	0.48 ± 0.10	[62]
24	SDSS DR10 and DR11	0.57	0.417 ± 0.045	[62]
25	SDSS-MGS	0.15	0.490 ± 0.145	[63]
26	SDSS-veloc	0.10	0.370 ± 0.130	[64]
27	FastSound	1.40	0.482 ± 0.116	[65]
28	SDSS-CMASS	0.59	0.488 ± 0.060	[66]
29	BOSS DR12	0.38	0.497 ± 0.045	[67]
30	BOSS DR12	0.51	0.458 ± 0.038	[67]
31	BOSS DR12	0.61	0.436 ± 0.034	[67]
32	BOSS DR12	0.38	0.477 ± 0.051	[68]
33	BOSS DR12	0.51	0.453 ± 0.050	[68]
34	BOSS DR12	0.61	0.410 ± 0.044	[68]
35	Vipers v7	0.76	0.440 ± 0.040	[69]
36	Vipers v7	1.05	0.280 ± 0.080	[69]
37	BOSS LOWZ	0.32	0.427 ± 0.056	[70]
38	BOSS CMASS	0.57	0.426 ± 0.029	[70]
39	Vipers	0.727	0.296 ± 0.0765	[71]
40	6dFGS+SnIa	0.02	0.428 ± 0.0465	[72]
41	Vipers	0.6	0.48 ± 0.12	[73]
42	Vipers	0.86	0.48 ± 0.10	[73]
43	Vipers PDR-2	0.60	0.550 ± 0.120	[74]
44	Vipers PDR-2	0.86	0.400 ± 0.110	[74]
45	SDSS DR13	0.1	0.48 ± 0.16	[75]
46	2MTF	0.001	0.505 ± 0.085	[76]
47	Vipers PDR-2	0.85	0.45 ± 0.11	[77]
48	BOSS DR12	0.31	0.469 ± 0.098	[78]
49	BOSS DR12	0.36	0.474 ± 0.097	[78]
50	BOSS DR12	0.40	0.473 ± 0.086	[78]
51	BOSS DR12	0.44	0.481 ± 0.076	[78]
52	BOSS DR12	0.48	0.482 ± 0.067	[78]
53	BOSS DR12	0.52	0.488 ± 0.065	[78]
54	BOSS DR12	0.56	0.482 ± 0.067	[78]
55	BOSS DR12	0.59	0.481 ± 0.066	[78]
56	BOSS DR12	0.64	0.486 ± 0.070	[78]
57	SDSS DR7	0.1	0.376 ± 0.038	[79]
58	SDSS-IV	1.52	0.420 ± 0.076	[80]
59	SDSS-IV	1.52	0.396 ± 0.079	[81]
60	SDSS-IV	0.978	0.379 ± 0.176	[82]
61	SDSS-IV	1.23	0.385 ± 0.099	[82]
62	SDSS-IV	1.526	0.342 ± 0.070	[82]
63	SDSS-IV	1.944	0.364 ± 0.106	[82]

TABLE IV. Hubbe parameter data [44].

Index	z	H	References
1	0.0708	69.0 ± 19.68	[83]
2	0.09	69.0 ± 12.0	[84]
3	0.12	68.6 ± 26.2	[83]
4	0.17	83.0 ± 8.0	[85]
5	0.179	75.0 ± 4.0	[86]
6	0.199	75.0 ± 5.0	[86]
7	0.20	72.9 ± 29.6	[83]
8	0.27	77.0 ± 14.0	[85]
9	0.28	88.8 ± 36.6	[83]
10	0.35	82.0 ± 4.85	[87]
11	0.352	83.0 ± 14.0	[88]
12	0.3802	83.0 ± 13.5	[88]
13	0.4	95.0 ± 17.0	[85]
14	0.4004	77.0 ± 10.2	[88]
15	0.4247	87.1 ± 11.2	[88]
16	0.4497	92.8 ± 12.9	[88]
17	0.4783	80.9 ± 9.0	[88]
18	0.48	97.0 ± 62.0	[89]
19	0.593	104.0 ± 13.0	[86]
20	0.68	92.0 ± 8.0	[86]
21	0.781	105.0 ± 12.0	[86]
22	0.875	125.0 ± 17.0	[86]
23	0.88	90.0 ± 40.0	[89]
24	0.9	117.0 ± 23.0	[85]
25	1.037	154.0 ± 12.0	[86]
26	1.3	168.0 ± 17.0	[85]
27	1.363	160.0 ± 33.6	[90]
28	1.43	177.0 ± 18.0	[85]
29	1.53	140.0 ± 14.0	[85]
30	1.75	202.0 ± 40.0	[85]
31	1.965	186.5 ± 50.4	[90]

-
- [1] Riess, A. G. et *al.*, *Astron. J.* **116**, 1009 (1998) [arXiv: 9805201 [astro-ph]].
 Riess, A. G. et *al.*, *Astron. J.* **117**, 707 (1999) [arXiv: 9810291 [astro-ph]].
 S. Perlmutter et *al.*, *Astrophys. J.* **515**, 565 (1999) [arXiv: 9812133 [astro-ph]].
- [2] D. N. Spergel et *al.*, [WMAP Collaboration], *astrophys. J. Suppl* **184**, 175 (2003) [arXiv:0302209 [astro-ph]].
- [3] P. A. R. Ade et *al.*, [Planck Collaboration], *Astron. Astrophys. J. Suppl.* **594**, A13 (2016) [arXiv:1502.01589 [astro-ph]].
- [4] N. Aghanim et *al.*, [Planck Collaboration], ‘Planck 2018 results. VI. Cosmological parameters’ [arXiv:1807.06209 [astro-ph.CO]].
- [5] P. J. Steinhardt, in *critical problems in Physics*, edit by V. L. Fitch and D. R. Marlow (Princeton University Press, Princeton, NJ, 1997).
- [6] S. Weinberg, *Rev. Mod. Phys.* **61**, 1(1989).
- [7] W. L. Freedman, *Nat. Astron.* **1**, 0169 (2017) [arXiv:1706.02739 [astro-ph.CO]].
- [8] J. L. Bernal, L. Verde, and A. G. Riess, *JCAP* **10**, 019 (2016) [arXiv:1607.05617 [astro-ph.CO]].
- [9] Adam G. Riess et *al.*, *Astrophys. J.* **861**, 126 (2018) [arXiv:1804.10655 [astro-ph.CO]].
- [10] Kenneth C. Wong et *al.*, [H0LiCOW collaboration], Submitted to *MNRAS* (2019) [arXiv:1907.0.4869 [astrp-ph.CO]].
- [11] B. Ratra, P. J. Peebles, *Phys. Rev. D* **37**, 3406 (1988).
- [12] T. Chiba, A. De Felice and S. Tsujikawa, *Phys. Rev. D* **87**, 083505 (2013) [arXiv:1210.3859 [astro-ph.CO]].
- [13] E. J. Copeland, M. Sami, and S. Tsujikawa, *Int. J. Mod. Phys. D* **15**, 1753 (2006) [arXiv:hep-th/0603057].
- [14] S. Tsujikawa, *Class. Quant. Grav.* **30**, 214003 (2013) [arXiv:1304.1961 [gr-qc]].
- [15] C. Armendariz-Picon, V. Mukhanov and P. J. Steinhardt, *Phys. Rev. Lett.* **85**, 4438 (2000) [arXiv:astro-ph/0004134].
- [16] C. Armendariz-Picon, V. Mukhanov and P. J. Steinhardt, *Phys. Rev. D* **63**, 103510 (2001) [arXiv:astro-ph/0006373].
- [17] C. Brans and R. Dicke, *Phys. Rev.* **124**, 925 (1961).
- [18] S. Tsujikawa, *Phys. Rev. D* **77**, 023507 (2008) [arXiv:0709.1391 [astro-ph]].
- [19] S. Tsujikawa, K. Uddin, S. Mizuno, R. Tavakol and J. Yokoyama, *Phys. Rev. D* **77**, 103009 (2008) [arXiv:0803.1106 [astro-ph]].
- [20] A. Nicolis, R. Rattazzi, and E. Trincherini, *Phys. Rev. D* **79**, 064036 (2009) [0811.2197 [hep-th]].
- [21] C. Deffayet, G. Esposito-Farese, and A. Vikman, *Phys. Rev. D* **79**, 084003 (2009) [arXiv:0901.1314 [hep-th]].
- [22] C. Deffayet, O. Pujolas, I. Sawicki, and A. Vikman, *JCAP* **1010** (2010) 026 [arXiv:1008.0048 [hep-th]].
- [23] T. Kobayashi, M. Yamaguchi, and J. Yokoyama, *Phys. Rev. Lett.* **105**, 231302 (2010) [arXiv:1008.0603 [hep-th]].
- [24] G. W. Horndeski, *Int. J. Theor. Phys.* **10** 363 (1974).
- [25] T. Kobayashi, *Rept. Prog. Phys.* **82**, no. 8, 086901 (2019) [arXiv:1901.07183 [gr-qc]].
- [26] S. Nesseris, A. De Felice and S. Tsujikawa, *Phys. Rev. D* **82**, 124054 (2010) [arXiv:1010.0407 [astro-ph.CO]].
- [27] A. De Felice and S. Tsujikawa, *Phys. Rev. Lett.* **105**, 111301 (2010). [arXiv:1007.2700 [astro-ph.CO]].
- [28] A. De Felice, S. Tsujikawa, *JCAP* **03**, 025 (2012) [arXiv:1112.1774 [astro-ph.CO]].
- [29] A. De Felice, S. Tsujikawa, *JCAP* **02**, 007 (2012) [arXiv:1110.3878 [gr-qc]].
- [30] A. De Felice, R. Kase, and S. Tsujikawa, *Phys. Rev. D* **83**, 043515 (2011) [arXiv:1011.6132 [astro-ph.CO]].

- [31] A. De Felice and S. Tsujikawa, *Phys. Rev. D* **84**, 124029 (2011) [arXiv:1008.4236 [hep-th]].
- [32] C. Leloup et al. *JCAP* **05**, 011 (2019) [arXiv:1902.07065 [astro-ph.CO]].
- [33] J. Neveu and al. *Astronomy & Astrophysics* **600**, A40 (2017) [arXiv:1605.02637 [gr-qc]].
- [34] J. Neveu and al. *Astronomy & Astrophysics* **555**, A53 (2013) [arXiv:1302.2786 [gr-qc]].
- [35] S. Peirone, G. Benevento, N. Frusciante and S. Tsujikawa, (2019) [arXiv:1905.05166].
- [36] R. Kase and S. Tsujikawa, *Phys. Rev. D* **97**, 103501 (2018) [arXiv:1802.02728 [gr-qc]].
- [37] A. Padilla, P.M. Saffin and S.-Y. Zhou, *JHEP* **12**, 031 (2010) [arXiv:1007.5424 [hep-th]].
- [38] T. Chiba, A. De Felice and S. Tsujikawa, *Phys. Rev. D* **90** (2), 023516 (2014) [arXiv:1405.3459 [gr-qc]].
- [39] D. Langlois, S. Renaux-Petel, D.A. Steer and T. Tanaka, *Phys. Rev. Lett.* **101**, 061301 (2008) [arXiv:0804.3139 [hep-th]].
- [40] A. Padilla and V. Sivanesan, *JHEP* **1304**, 032 (2013) [arXiv:1210.4026 [gr-qc]].
- [41] T. Kobayashi, N. Tanahashi and M. Yamaguchi, *Phys. Rev. D* **88**, 083504 (2013) [arXiv:1308.4798 [hep-th]].
- [42] L. Kazantzidis and L. Perivolaropoulos. *Phys. Rev. D* **97**, 103503 (2018) [arXiv:1803.01337 [astro-ph.CO]].
- [43] S. Nesseris, G. Pantazis and L. Perivolaropoulos. *Phys. Rev. D* **96**, 023542 (2017) [arXiv:1703.10538 [astro-ph.CO]].
- [44] R. Jimenez and A. Loeb, *Astrophys. J.* **573**, 37 (2002) [arXiv:0106145 [astro-ph]].
- [45] H. Hildebrandt et al., *Mont. Not. Roy. Astron. Soc.* **465**, 1454 (2017) [arXiv:1606.05338 [astro-ph.CO]].
- [46] T. M. C. Abbott et al., [DES collaboration], *Phys. Rev. D* **98**, 043526 (2018) [arXiv:1708.01530 [astro-ph.CO]].
- [47] Bruno J. Barros et al., *JCAP* **01**, 007 (2019) [arXiv:1802.09216v2 [astro-ph.CO]].
- [48] Caroline D. Huang et al., Submitted to *ApJ* [arXiv:1908.10883 [astro-ph.SR]].
- [49] Wendy L. Freedman et al., [arXiv:1907.05922v1 [astro-ph.CO]].
- [50] R. E. Kass and A. E. Raftery, *J. Am. Stat. Assoc.* **90**, 773 (1995).
- [51] Y. Song and W. J. Percival, *JCAP* **10**, 004 (2009) [arXiv:0807.0810 [astro-ph]].
- [52] M. Davis et al, *Mon. Not. Roy. Astron. Soc.* **413**, 2906 (2011) [arXiv:1011.3114 [astro-ph.CO]].
- [53] M. J. Hudson and S. J. Turnbull, *ApJL* **751**, L30 (2012) [arXiv:1203.4814 [astro-ph.CO]].
- [54] S. J. Turnbull, et al., *Mon. Not. Roy. Astron. Soc.* **420**, 447 (2012) [arXiv:1111.0631 [astro-ph.CO]].
- [55] L. Samushia, W. J. Percival and A. Raccanelli, *Mon. Not. Roy. Astron. Soc.* **420**, 2102 (2012) [arXiv:1102.1014 [astro-ph.CO]].
- [56] C. Blake et al., *Mon. Not. Roy. Astron. Soc.* **425**, 405 (2012) [arXiv:1204.3674 [astro-ph.CO]].
- [57] F. Beutler et al., *Mon. Not. Roy. Astron. Soc.* **423**, 3430 (2012) [arXiv:1204.4725 [astro-ph]].
- [58] R. Tojeiro et al., *Mon. Not. Roy. Astron. Soc.* **424**, 2339 (2012) [arXiv:1203.6565 [astro-ph.CO]].
- [59] S. de la Torre et al., *Astron. Astrophys.* **557**, A54 (2013), [arXiv:1303.2622 [astro-ph.CO]].
- [60] C. Chuang and Y. Wang, *Mon. Not. Roy. Astron. Soc.* **435**, 255 (2013) [arXiv:1209.0210 [astro-ph.CO]].
- [61] C. Blake et al., *Mon. Not. Roy. Astron. Soc.* **436**, 3089 (2013), [arXiv:1309.5556 [astro-ph.CO]].
- [62] A. G. Sanchez et al., *Mon. Not. Roy. Astron. Soc.* **440**, 2692-2713 (2014), [arXiv:1312.4854 [astro-ph.CO]].
- [63] S. N. Howlett et al., *Mon. Not. Roy. Astron. Soc.* **449**, 848-866 (2015) [arXiv:1409.3238 [astro-ph.CO]].
- [64] M. Feix, A. Nusser, and E. Branchini, *Phys. Rev. Lett.* **115**, 011301 (2015) [arXiv:1503.05945 [astro-ph.CO]].
- [65] T. Okumura et al., *Publ. Astron. Soc. Jap.* **68**, 24 (2016) [arXiv:1511.08083 [astro-ph.CO]].
- [66] C. Chuang et al., *Mon. Not. Roy. Astron. Soc.* **461**, 3781-3793 (2016) [arXiv:1312.4889 [astro-ph.CO]].
- [67] S. Alam et al., (BOSS), *Mon. Not. Roy. Astron. Soc.* **470**, 2617-2652 (2017) [arXiv:1607.03155 [astro-ph.CO]].
- [68] F. Beutler et al. (BOSS), *Mon. Not. Roy. Astron. Soc.* **466**, 2242-2260 (2017) [arXiv:1607.03150 [astro-ph.CO]].
- [69] N. Padmanabhan and M. J. White, *Phys. Rev. D* **77**, 123540 (2008) [arXiv:0804.0799 [astro-ph]].
- [70] H. Gil-Marn et al., *Mon. Not. Roy. Astron. Soc.* **465** no. 2, 1757 (2017) [arXiv:1606.00439 [astro-ph.CO]].
- [71] A. J. Hawken et al., *Astron. Astrophys.* **607**, A54 (2017) [arXiv:1611.07046 [astro-ph.CO]].
- [72] D. Huterer, D. Shafer, D. Scolnic, and F. Schmidt, *JCAP* **05**, 015 (2017) [arXiv:1611.09862 [astro-ph.CO]].
- [73] S. de la Torre et al., *Astron. Astrophys.* **608**, A44 (2017) [arXiv:1612.05647 [astro-ph.CO]].
- [74] A. Pezzotta et al., *Astron. Astrophys.* **604**, A33 (2017) [arXiv:1612.05645 [astro-ph.CO]].
- [75] M. Feix, E. Branchini, and A. Nusser, *Mon. Not. Roy. Astron. Soc.* **468**, 1420 (2017) [arXiv:1612.07809 [astro-ph.CO]].
- [76] C. Howlett et al., *Mon. Not. Roy. Astron. Soc.* **471**, 3135 (2017) [arXiv:1706.05130 [astro-ph.CO]].
- [77] F. G. Mohammad et al., *Astron. Astrophys.* **606**, A59 (2018) [arXiv:1708.00026 [astro-ph.CO]].
- [78] Y. Wang et al., *Mon. Not. R. Astron. Soc.* **481**, no. 3, 3160 (2018) [arXiv:1709.05173 [astro-ph.CO]].
- [79] F. Shi et al., *The Astrophysical Journal* **861**, 137 (2018) [arXiv:1712.04163 [astro-ph.CO]].
- [80] H. Gil-Marn et al., *Mon. Not. Roy. Astron. Soc.* **477**, no. 2, 1604 (2018) [arXiv:1801.02689 [astro-ph.CO]].
- [81] J. Hou et al., *Mon. Not. Roy. Astron. Soc.* **480**, no. 2, 2521 (2018) [arXiv:1801.02656 [astro-ph.CO]].
- [82] G. Zhao et al., *Mon. Not. Roy. Astron. Soc.* **482**, no. 3, 3497 (2019) [arXiv:1801.03043 [astro-ph.CO]].
- [83] C. Zhang et al., *Res. Astron. Astrophys.* **14**, 1221 (2014) [arXiv:1207.4541 [astro-ph.CO]].
- [84] R. Jimenez, A. Loeb, *Astrophys. J.* **573**, 37 (2002) [arXiv:0106145 [astro-ph]].
- [85] J. Simon, L. Verde, R. Jimenez, *Phys. Rev. D* **71**, 123001 (2005) [arXiv:0412269 [astro-ph]].
- [86] M. Moresco et al., *J. Cosmol. Astropart. Phys.* **8**, 006 (2012) [arXiv:1201.3609 [astro-ph.CO]].
- [87] C.-H. Chuang et al., *Mon. Not. R. Astron. Soc.* **426**, 226 (2012) [arXiv:1102.2251 [astro-ph.CO]].
- [88] M. Moresco et al., *JCAP* **05**, 014 (2016) [arXiv:1601.01701v2 [astro-ph.CO]].
- [89] D. Stern, R. Jimenez, L. Verde, S. A. Stanford and M. Kamionkowski, *Astrophys. J. Suppl.* **188**, 280 (2010) [arXiv:0907.3152 [astro-ph.CO]].
- [90] M. Moresco, *Mon. Not. R. Astron. Soc.* **450**, L16 (2015) [arXiv:1503.01116 [astro-ph.CO]].